PPPL-2021

DIELECTRONIC SATELLITE SPECTRA OF HYDROGENLIKE TITANIUM (Ti XXII)

By

M. Bitter et al.

JULY 1983

PLASMA PHYSICS LABORATORY

PRINCETON UNIVERSITY
PRINCETON, NEW JERSEY

PREPARED FOR THE U.S. DEPARTMENT OF ENERGY, UNDER CONTRACT DE-AC02-76-CHO-3073.

DISCLAIMER

NOTICE

Printed in the United States of America.

Available from:

National Technical Information Service
U. S. Department of Commerce
5285 Port Royal Road
Springfield, Virginia 22151

Price: Printed Copy $ * ; Microfische $3.50

*PAGES	NTIS Selling Price
1-25	$5.00
26-50	$6.50
51-75	$8.00
76-100	$9.50
101-125	$11.00
126-150	$12.50
151-175	$14.00
176-200	$15.50
201-225	$17.00
226-250	$18.50
251-275	$20.00
276-300	$21.50
301-325	$23.00
326-350	$24.50
351-375	$26.00
376-400	$27.50
401-425	$29.00
426-450	$30.50
451-475	$32.00
476-500	$33.50
500-525	$35.00
526-550	$36.50
551-575	$38.00
576-600	$39.50

For documents over 600 pages, add $1.50 for each additional 25 page increment.

DIELECTRONIC SATELLITE SPECTRA OF HYDROGENLIKE TITANIUM (Ti XXII)

PPPL--2021

DE83 017984

July 1983

M. Bitter, S. von Goeler, S. Cohen, K. W. Hill
S. Sesnic, F. Tenney, and J. Timberlake

Plasma Physics Laboratory, Princeton University
Princeton, New Jersey 08544

U. I. Safronova
Institute for Spectroscopy
Troitsk, Podolsky District 142092, USSR

L. A. Vainshtein
Lebedev Physical Institute, Moscow 117924, USSR

J. Dubau and M. Loulergue
Observatoire de Meudon, 92190 Meudon, France

F. Bely-Dubau and L. Steenman-Clark
Observatoire de Nice, Boite Postale No. 252,06007
Nice Cedex, France

ABSTRACT

High resolution spectra of the $Ly\alpha_1$ and $Ly\alpha_2$ lines of hydrogenlike titanium, TiXXII, and the associated dielectronic satellites which are due to transitions $1snl-2pnl$ with $n \geq 2$, have been observed from tokamak discharges with auxiliary ion cyclotron heating (ICRH) with central electron temperatures of 2 keV and central electron densities of $8 \times 10^{13}\text{cm}^{-3}$ on the Princeton Large Torus (PLT). The data have been used for a detailed comparison with theoretical predictions based on the Z – expansion method[29] and Hartree – Fock calculations.[3] The results obtained with the Z – expansion method are in excellent agreement with the observed spectral data except for minor discrepancies between the theoretical and experimental wavelengths of 0.0003 Å for the $n = 2$ satellites and of 0.0001 Å for the separation of the $Ly\alpha_1$ and $Ly\alpha_2$ lines. Very good agreement with the experimental data is also obtained for the results from the Hartree – Fock calculations though somewhat larger discrepancies ($\simeq$ 0.0009 Å) exist between experimental and theoretical wavelengths which are systematically too small. The observed spectra are used for diagnosis of the central ion and electron temperatures of the PLT discharges and for a measurement of the dielectronic recombination rate coefficient of Ti XXII. The measured rate coefficient is in good agreement with both the predictions from the detailed calculations (Safronova and Vainshtein, and Dubau et al.) and of Burgess' general formula.[39]

I. INTRODUCTION

Spectra of hydrogenlike titanium, Ti XXII, are presented in this paper. The spectra have been observed from tokamak discharges with central electron temperatures in excess of 2 keV on the Princeton Large Torus (PLT) using a high resolution crystal spectrometer. The good spectral resolution and the high electron temperatures produced by ion cyclotron resonance heating (ICRH) have allowed detailed experimental data on the dielectronic satellites of the $Ly\alpha_1$ and $Ly\alpha_2$ lines of Ti XXII to be obtained for the first time and also permitted a detailed comparison with the theories by Safronova and Vainshtein[1,2] and Dubau et al.[3,4] to be performed. The spectra have also been used for measurements of the central ion and electron temperature in the hot core of PLT discharges and for a determination of the dielectronic recombination rate coefficient of Ti XXII.

The spectra of hydrogenlike ions are of fundamental importance for the study of multiply charged heavy ions. This is true, in particular, with regard to relativistic effects which are most evident from the fine structure splitting of the $1s - 2p$ resonance line. The resonance line splitting strongly increases with atomic number Z. Whereas the separation of the fine structure components of the resonance lines of low-Z hydrogenlike ions is very small and usually masked by Doppler broadening, the doublet is well-resolved for ions, such as Ti XXII. For exact wavelength calculations it is necessary to also include QED effects due to self-energy and vacuum-polarization, such as the Lamb shift.[5]

In addition to the resonance lines, the spectra of high-Z hydrogenlike

ions show a series of dielectronic satellites which are due to transitions of the type $1snl - 2pnl$ with $n \geq 2$. The $2pnl$ states are doubly excited heliumlike states above the ionization limit of the heliumlike ion. These states can autoionize to the hydrogenlike ground state, or they can decay by a stabilizing radiative transition to a singly excited heliumlike state. The latter transition gives rise to a satellite line. Since the radiative decay probability increases with Z^4, whereas the autoionization probability is approximately independent of Z, the satellite lines are relatively intense compared with the resonance line only for ions with $Z \geq 20$. In low density plasmas the $2pnl$ states are not populated from the heliumlike $1s^2$ ground state, since double collisions are highly improbable. The satellites can, therefore, only be produced by the dielectronic recombination of hydrogenlike ions. This is different for the previously well-documented satellite spectra of heliumlike ions,[6,7,8,9,10,11] where dielectronic recombination and collisional inner shell excitation are equally important. The satellite spectra of hydrogenlike ions observed from low density plasmas are, therefore, of great interest for a study of the dielectronic recombination process. Spectra of the $Ly\alpha_1$ and the $Ly\alpha_2$ lines and their associated satellites are presently also studied in beam – foil experiments.[12,13] The excitation mechanisms for the satellite lines are, however, less well-defined in these experiments than for low density plasmas.[14]

Tokamak plasmas are presently the best suited laboratory plasmas for observation of the line spectra from highly ionized ions. In fact, it is now possible to obtain large volume tokamak plasmas with central electron densities of $0.1 - 1 \times 10^{15}\,\mathrm{cm}^{-3}$ and electron temperatures in the range from 1 to 3

keV under quasi-steady-state conditions for periods of 100 – 300 msec. Under these conditions the relative abundance and spatial distribution of the different states of ionization of high-Z elements approximate coronal equilibrium. Since tokamak plasmas are also the best diagnosed high temperature plasmas, they are appropriate for experimental testing of atomic theories concerning the spectra of multiply charged ions. On the other hand, the spectra of high-Z ions will be of increasing importance for diagnosis of central plasma parameters in the the next generation of large tokamaks, for which central electron and ion temperatures in excess of 10 keV are predicted. In particular, determination of the central ion temperature from Doppler broadening of the resonance lines of hydrogenlike ions with $Z \geq 20$ will be of vital importance for future tokamak experiments.

II. EXPERIMENTAL SETUP

Hydrogenlike titanium, Ti XXII, can be produced in hot plasmas under coronal equilibrium conditions[15] with a fractional abundance of 10 $^0/_0$ if the electron temperature exceeds 2 keV (see Fig. 1). Plasmas of sufficiently high electron temperatures are presently obtained in the core of large tokamaks with use of additional heating schemes. Nevertheless, it is experimentally difficult to produce these ions in appreciable amounts, since significant deviations from the ideal charge state distribution are observed in tokamak plasmas as a result of the radial particle transport.[16] Coronal equilibrium is only approached if the characteristic confinement time of an ion is long compared with the ionization and recombination times.[17,18] This condition is especially hard to fulfill for hydrogenlike ions, because the ionization and recombination times are con-

siderably longer for these ions than for ions of the lower charge states. This is due to the high ionization potential of the heliumlike ions (E_I = 6.249 keV for Ti XXI) and due to the fact that dielectronic recombination – the dominant mechanism of recombination for ions below the heliumlike charge state – is comparatively unimportant. Since the confinement time increases with plasma density, whereas the recombination and ionization times are inversely proportional to the electron density, the most efficient way to enhance the concentration of hydrogenlike ions is to perform the experiments at high plasma densities.

In PLT discharges with additional ion cyclotron heating (ICRF) of 4 MW at 25 MHz it has been possible to produce plasmas with central electron densities of $\simeq 1 \times 10^{14} \mathrm{cm}^{-3}$ and central electron temperatures of 2 - 3 keV with a minor radius of 40 cm in quasi-steady-state for periods of 200 - 300 msec. Even under these conditions the characteristic time for radial transport of hydrogenlike titanium ions as determined from titanium injection experiments was only about one third the ionization time ($\simeq$100 msec) of the heliumlike Ti XXI ions.[19] Transport was, therefore, important in our experiments. We may assume that the radial density profile of the Ti XXII ions was wider and the relative abundance of the Ti XXII and Ti XXI charge states in the center of the plasma was smaller than the coronal equilibrium values, shown in Fig. 1, although we did not measure these radial ion charge state distributions. A further experimental difficulty arises from the fact that the dielectronic satellite lines are relatively intense only at low electron temperatures. The spectra of greatest interest are, therefore, emitted at temperatures for which the hydrogenlike ions are not the most abundant charge state. Under these conditions the background radiation

from the bremsstrahlung and the radiative recombination continuum can be comparable or even larger than the observed line radiation, and it is, therefore, difficult to obtain spectra with a small statistical error.

Titanium is used on the PLT tokamak as a material for the Faraday shields of the rf – antennas and as a getter for low-Z impurities. During the ohmic heating phase with electron temperatures of 1 to 1.5 keV the line radiation from hydrogenlike titanium, Ti XXII, is smaller than the background radiation. With rf – heating it is, however, enhanced due to both an increase in the amount of titanium in the discharge and an increase in the central electron temperature. Most of the data have, therefore, been taken under these conditions. In a series of discharges the titanium concentration has been increased by injection of titanium using the laser blowoff technique.[20] In these experiments a controlled amount of titanium was induced by directing a laser beam of adjustable cross – section and power against a titanium target. This technique also permitted to identify unambiguously the observed radiation as titanium lines.

The data were recorded by a high resolution ($\lambda/\Delta\lambda = 15000$, at λ=2.5 Å) curved crystal spectrometer which permitted simultaneous observation of spectrum lines in the wavelength range from 2.485 Å to 2.525 Å. The spectrometer consisted of a ($20\bar{2}3$; $2d = 2.7497$ Å) quartz crystal and a position sensitive multiwire proportional counter[21] in the Johann configuration.[22] The dimensions of the crystal and its radius of curvature were 6" × 1.5" × 0.030" and 369.5 cm, respectively. The spectrometer is very similar to the one previously used for observation of the dielectronic satellite spectrum of heliumlike titanium, Ti XXI,[11] and Doppler broadening measurements on the PDX (Poloidal Divertor

Experiment) tokamak.[23] Instrumental details have been described in reference .[24]

Figure 2 shows spectra accumulated from 17 PLT discharges during consecutive time intervals from 600 – 650 msec and 650 – 700 msec. Ion cyclotron heating of 4 MW was applied during the period from 500 – 700 msec, and titanium was injected at the time of 650 msec. The line radiation is consequently enhanced by about a factor of two in the spectrum of Fig. 2b, which was obtained immediately after the titanium injection. Typical profiles of the laser Thomson scattering data for these PLT discharges exhibiting a central electron temperature of 2 keV and a central electron density of $8 \times 10^{13} cm^{-3}$ are shown in Fig. 3. In addition to the Ti XXII line radiation the spectra in Fig. 2 show a relatively intense background from the radiation continuum. An approximate number of 1.5×10^{17} titanium atoms was injected into each discharge. Some data were taken with an improved time resolution of 15 msec to study the time history of the Ti XXII spectrum lines. From these measurements we deduced a value of 20 – 30 msec for the confinement time of the Ti XXII ions. The titanium injection experiments have also allowed us to obtain an estimate of the total number of titanium atoms that are normally present in the discharge from the Faraday shields and the titanium gettering. By comparing the intensities of the titanium line radiation observed before and immediately after injection we conclude that the titanium supply from these sources was comparable with the injected titanium.

In order to reduce the statistical error and to distinguish clearly the Ti XXII and Ti XXI spectral features from the background radiation, the spectrum, shown in Fig. 4, was accumulated from 78 rf heated PLT discharges with almost

identical parameters. The dashed line between B and D indicates the background level of the radiation continuum. The background is constant except for a slight reduction observed at the lower channel numbers. This intensity reduction, which is less than 5 $^{0}/_{0}$ in the immediate vicinity of spectral feature 1, is caused by a vignetting effect of the beryllium window on the PLT tokamak. For a detailed comparison with theoretical predictions the data points at the channel numbers from 87 to 145 have been corrected for this geometrical effect. The intensity correction factors were determined from a linear interpolation of the background radiation represented by the dashed line between A and C.

III. EXPERIMENTAL RESULTS AND THEORETICAL PREDICTIONS

Spectra of hydrogenlike ions have been previously observed from solar flares and from tokamak plasmas for $Z \preceq 20$.[25,26,27] These observations have well–confirmed the predicted Z – dependence both for the doublet splitting of the resonance line and the intensity of the dielectronic satellites. The Z – dependence of these spectral features is illustrated in Fig. 5 which presents spectra of hydrogenlike ions for Z = 8, 12, 16, and 20. For O VIII and Mg XII the separation of the Lyα doublet is smaller than the Doppler width, whereas for S XVI and Ca XX the fine structure components of the resonance line are clearly resolved. Similarly, the 1snl – 2pnl dielectronic satellites are not observed in the spectra of O VIII and Mg XII. They appear in the spectrum of S XVI, and are clearly noticeable in the solar flare spectrum of Ca XX. However, the statistical error of these data has not permitted a detailed comparison with theoretical predictions. An interesting result is the observation of intensity ratios in the range from 0.5 to

0.8 for the $Ly\alpha_2$ and the $Ly\alpha_1$ lines of S XVI on the ALCATOR experiment.[26] This departure from the value of 0.5 has been ascribed to excitation of the $2P_{3/2}$ and $2P_{1/2}$ states from the metastable $2S_{1/2}$ state by proton collisions.[28]

In this section we give a detailed comparison of the observed Ti XXII spectra with theoretical predictions of Safronova and Vainshtein[2] and Dubau et al.[4] At present two methods are used to calculate atomic parameters (wavelengths, autoionization and radiative transition probabilities) for dielectronic satellites: the Z – expansion method of Safronova and Vainshtein,[29] and the Hartree – Fock approach which is employed by Dubau et al.[3,30] A comparison of the results obtained by these different methods of calculation with experimental data is of great interest for the theory of multiply charged high–Z ions. Table I lists the experimental wavelengths and theoretical results for the most prominent spectral features which have been identified as the $1s(^2S_{1/2}) - 2p(^2P_{3/2})$ and the $1s(^2S_{1/2}) - 2p(^2P_{1/2})$ fine structure components of the resonance transition, or the Lyα_1 and the Lyα_2 lines (features 1 and 2), and the well–resolved $1snl - 2pnl$ dielectronic satellites with $n = 2$ (features 3 – 8). The experimental wavelengths have been determined relative to the Lyα_2 line for which we adopted the theoretical value of 2.4957 Å.[1] Structures observed on the wings of the Lyα_1 and the Lyα_2 lines are ascribed to $1snl - 2pnl$ dielectronic satellites with $n \geq 3$. Contrary to the $n = 2$ satellites, the $n \geq 3$ satellites can be uniquely assigned to one of the fine structure components as the parent line, due to the fact that the electrostatic interaction between the $2p$ electron and the nl spectator electron, which is responsible for the satellite to resonance line separation, scales

as n^{-3} and is smaller than the $2p$ spin – orbit interaction if $n \geq 3$.[3] The Lyα_1 and the Lyα_2 lines thus represent the series limits for these satellites which are approached with increasing main quantum number n for the spectator electron. The number of satellite transitions increases dramatically with n. However, since the autoionization probability, Γ, decreases with n as n^{-3} and, moreover, $\Gamma \to 0$ for $\Delta n = 1$ transitions if $l \geq 2$,[31,32] the satellite intensity also decreases with n. Detailed calculations of the atomic parameters for all the $1snl - 2pnl$ transitions, which can be associated with the spectator electron in a certain n – shell, are usually performed for n – values up to five. The $n \geq 5$ satellites are then obtained by a line by line extrapolation from a selected set of $n = 5$ satellites with use of the appropriate scaling laws.[32] Tables II – IV list the theoretical predictions for satellites with $n = 3-5$ by Safronova and Vainshtein[2] and Dubau et al.[4] Included in the Tables are only the most intense transitions with line factors $Q_D \geq 5 \times 10^{11} \text{sec}^{-1}$. Since the satellites with $n \geq 3$ fall into a very narrow wavelength range and are partially blended with the resonance line, a detailed comparison between experiment and theory can only be made by use of synthetic spectra.

Figures 6 and 7 present the experimental data and synthetic spectra (solid lines) which have been obtained by calculating Voigt profiles for the transition arrays given in Tables I – IV. In addition to the fine structure components $1s(^2S_{1/2}) - 2p(^2P_{3/2})$ and $1s(^2S_{1/2}) - 2p(^2P_{1/2})$ of the Ti XXII resonance line, the theoretical spectra thus include the contribution from 14 $n = 2$ satellites (curve II), 49 $n = 3$ satellites (curve III), 47 $n = 4$ satellites (curve IV), and 38 $n = 5$ satellites (curve V). Curve I represents the total intensity of all these spectrum lines. For calculation of the synthetic spectra an intensity ratio of two

was assumed for the fine structure components of the Ti XXII resonance line, since excitation of the $2P_{3/2}$ and the $2P_{1/2}$ states from the $2S_{1/2}$ state by proton collisions are negligible at the plasma densities obtained in PLT discharges.[28] The intensities, i_d, of the satellites relative to the intensity of the resonance line have been obtained using the expression given by Safronova and Vainshtein[1] for the zero density limit:

$$i_d = \frac{3.836 \times 10^{-3}}{T_e} \exp\left(\frac{E_0 - E_s^{(n)}}{T_e}\right) \frac{0.24 + E_0/T_e}{1 + E_0/T_e} Q_D(\gamma, \gamma') \qquad (1)$$

where T_e is the electron temperature in keV. $E_0 = 4.939$keV is the energy of the Ti XXII resonance transition, and $E_s^{(n)} = 3.429, 4.273, 4.564,$ and4.699 keV, respectively, is the average energy of the autoionizing heliumlike states of a given n – shell relative to the hydrogenlike ground state. The line factor $Q_D(\gamma, \gamma')$ is defined as:

$$g_\gamma \frac{A(\gamma, \gamma')\Gamma(\gamma, \alpha_0)}{\Gamma(\gamma, \alpha_0) + \Sigma_{\gamma'} A(\gamma, \gamma')}$$

where g_γ is the statistical weight of the doubly excited heliumlike state γ. $\Gamma(\gamma, \alpha_0)$ is the probability for autoionization of the state γ to the hydrogenlike ground state α_0. $A(\gamma, \gamma')$ is the probability for the stabilizing radiative transition $\gamma - \gamma'$ of the heliumlike ion which gives rise to the satellite line, and $\Sigma_{\gamma'} A(\gamma, \gamma')$ is the total radiative decay probability for the state γ. $A(\gamma, \gamma')$, $\Gamma(\gamma, \alpha_0)$, and $Q_D(\gamma, \gamma')$ are in units of 10^{13}sec^{-1}. In order to obtain a best fit with the experimental data, the ion and electron temperatures were chosen to be $T_i = 1.8$ keV and $T_e = 2.1$ keV. The theoretical spectrum also includes the contribution of the magnetic dipole transition from $2S_{1/2}$ to $1S_{1/2}$ which is not strictly forbidden,[33] though the dominant decay of the $2S_{1/2}$ state is a two photon

process. Rate coefficients for the magnetic dipole transition (M1) and the two photon (2E1) decay of the $2S_{1/2}$ state have been derived by Breit and Teller,[34] and Drake,[35] who obtained the following results:

$$A_{M1} = 2.496 \times 10^{-6} Z^{10} \text{sec}^{-1}$$

$$A_{2E1} = 8.228 Z^{6} \text{sec}^{-1}$$

Because of the different Z dependences of these decay processes, the $M1$ transition becomes important for ions with $Z \geq 20$. The intensity ratio of the M1 line and the $Ly\alpha_2$ line is given by the expression

$$\frac{I(M1)}{I(Ly\alpha_2)} = c \times \frac{A(M1)}{A(M1) + A(2E1)} \tag{2}$$

where $c = 0.63$ (for $T_e = 2\text{keV}$) is the ratio of the excitation rates of the $2S_{1/2}$ and the $2P_{1/2}$ states from the $1S_{1/2}$ ground state.[1] From this expression we obtain for $I(M1)/I(Ly\alpha_2)$ a value of 0.04. The $M1$ line is separated from the $Ly\alpha_2$ line by the Lamb shift, which is 0.164 mÅ for Ti XXII.[5] This value is small compared with the Doppler width ($\simeq 1m\text{Å}$), and the $M1$ line is, therefore, not resolved in the observed Ti XXII spectrum.

Figures 6a and 6b show the experimental data and the synthetic spectra obtained from the predictions of Dubau et al.[4] (Table I and Tables IIb – IVb) and Safronova and Vainshtein[2] (Table I and Tables IIa – IVa), respectively. The theoretical spectra are in very good agreement with the experimental data. This is true, in particular, with regard to the relative satellite and resonance line intensities. Only small discrepancies are observed between theoretical and experimental wavelengths. These discrepancies are larger for the data of Dubau

et al.($\simeq 0.0009\mathring{A}$) than for those of Safronova and Vainshtein($\simeq 0.0003\mathring{A}$). The almost perfect fit to the data, which is shown in Fig. 6c, has been obtained by reducing the theoretical wavelengths of Safronova and Vainshstein for the $n = 2$ satellites by the constant amount of 0.0003 Å and using the value of 2.4903 Å (instead of Safronova's value of 2.4904 Å) for the wavelength of the $Ly\alpha_2$ line.

Figures 7a and 7b present the spectral range from 2.4850 Å to 2.5025 Å of Figs. 6b and 6c on an enlarged scale to allow for a more detailed comparison of the experimental data with the theoretical predictions for the fine structure components of the Ti XXII resonance line and the associated $n \geq 3$ satellites. The predicted (apparent) intensity profile of the $Ly\alpha_2$ line is in excellent agreement with the observation. However, a small discrepancy between theory and experiment exists on the long wavelength side of the $Ly\alpha_1$ line in Fig. 7a. In Fig. 7b this discrepancy has been largely removed by use of the corrected wavelength value of 2.4903 Å. We thus obtain the value of 0.0054 Å for the separation of the fine structure components of the Ti XXII resonance line. This value for the doublet separation is in very good agreement with Erickson's calculations who obtained 2.49122 Å and 2.49664 Å for the $Ly\alpha_1$ and the $Ly\alpha_2$ line, respectively.[5]

IV. DIAGNOSTIC APPLICATIONS

The satellite spectra of hydrogenlike ions are important for the diagnosis of hot plasmas. The main diagnostic applications are measurements of the ion and electron temperatures which can be determined from the Doppler broadening of spectrum lines and from the relative intensities of the resonance

line and the associated dielectronic satellites. Of particular interest are the spectra of hydrogenlike ions with $Z \geq 20$ for measurements of the central ion temperature in next generation of large tokamaks with expected core ion and electron temperatures in excess of 10 keV. Under these conditions impurity ions with $Z \preceq 20$ will be fully stripped in the hot center of the plasma, whereas ions with $Z \geq 20$ will predominantly be in the hydrogenlike charge state. The ion temperature in the hot core of the plasma can thus be obtained from Doppler broadening measurements of the resonance lines of these ions. In fact, Doppler broadening measurements of $Ly\alpha$ lines may be the most important central ion temperature diagnostic for these tokamaks since determination of the central ion temperature by standard techniques, such as the measurement of charge exchange neutrals, will be prevented by the projected large plasma density and plasma radius. The ion and electron temperature results obtained from evaluation of the Ti XXII spectra are shown in Figs. 8 and 9.

Figure 8 shows the value for the satellite to resonance line ratio, I_J/I_R, for the most prominent satellite J, as observed from the spectrum in Fig. 4, versus the experimental value of the central electron temperature and, for comparison, the predicted electron temperature dependence given by Eq. (1). The predictions and the experimental data are in agreement to within the experimental errors. According to the theoretical predictions the intensity ratio, I_J/I_R, is very sensitive to the electron temperature (solid line in Fig. 8). From these predictions we may infer that the intensity ratio, I_J/I_R, can be used as an electron temperature diagnostic up to values of $T_e = 3$ keV. For higher electron temperatures the intensity ratio, I_J/I_R, is smaller than 10 $^0/_0$, and it becomes

experimentally difficult to determine this ratio with sufficient accuracy.

The ion temperature has been determined from the apparent profile of the $Ly\alpha_2$ line. As discussed in Sec. III this line structure also includes the contribution from the $n \geq 3$ satellites associated with the $1s(^2S_{1/2}) - 2p(^2P_{1/2})$ transition. The satellites with $n = 3$ are the most intense and mainly contribute to the intensity in the wings of the resonance line profile. In principle, the ion temperature has to be evaluated by a fit of the experimental data with a synthetic spectrum which includes the contribution from all the satellites. However, this procedure requires elaborate computations which may be prohibitive for a fast evaluation of the ion temperature needed in tokamak experiments. We have, therefore, compared the ion temperature results which we obtained from a fit of the complete line structure to the experimental data (e.g., see Fig. 7b) with those obtained from the fit of a single Voigt function. Figure 9 shows the observed (apparent) $Ly\alpha_2$ line profiles of the spectra in Figs. 2a and 2b and the least squares fits of single Voigt profiles (solid lines) which were calculated with use of the plasma dispersion function as described in reference.[24] The arrows indicate the spectral range which has been used for the fit. The fitting limits have been chosen to exclude most of the wing structure due to the $n = 3$ satellites. The ion temperature values of $T_i = 2.0 \pm 0.2$ keV and $T_i = 1.8 \pm 0.1$ keV obtained from a single Voigt function fit to the data in Figs. 9a and 9b, respectively, were practically identical with the T_i - values derived from the fit to the complete line structure. As the electron temperature increases above 3 keV, it is expected that the intensity of the $n \geq 3$ satellites rapidly decreases and that the observed line profile resembles more and more a single Voigt profile.

V. MEASURENENT OF THE DIELECTRONIC RECOMBINATION RATE COEFFICIENT OF Ti XXII

The dielectronic recombination rate coefficient, α_d, can be written in the form[32]

$$\alpha_d = C_R(T_e)\Sigma_s I_s/I_R$$

where $\Sigma_s I_s/I_R$ is the total intensity of all the dielectronic satellites relative to the intensity of the resonance line, and $C_R(T_e)$ is the collisional excitation rate coefficient for the resonance transition. The dielectronic recombination rate coefficient, α_d, can thus be experimentally determined from a measurement of the total relative satellite intensity, $\Sigma_s I_s/I_R$, if the excitation rate coefficient, $C_R(T_e)$, is known. These coefficients have been calculated for the heliumlike and hydrogenlike resonance lines by Safronova and Vainshtein.[1]

Since the intensities of the resonance line and the associated dielectronic satellites are proportional to the abundance of the ions of a single charge state, the experimental results on α_d are independent of the ionization state of the plasma. Plasma modeling calculations[36] are, therefore, not necessary. So far, this experimental method has been used to determine the dielectronic recombination rate coefficients for the heliumlike charge states of titanium, Ti XXI,[37] and iron, Fe XXV.[38] Satellites to the heliumlike resonance lines are due to transitions of the type $1s^2nl - 1s2pnl$ with $n \geq 2$. These satellites are produced by the process of dielectronic recombination as well as by collisional inner shell excitation of lithiumlike ions in the $1s^22s$ ground state. Appropriate corrections for the latter contribution are, therefore, necessary, for a measurement of the

dielectronic recombination rate coefficient from lithiumlike satellites. On the other hand, the heliumlike $1snl-2pnl$ (with $n \geq 2$) satellites of the hydrogenlike resonance lines are entirely produced in the process of dielectronic recombination and are, therefore, of principal importance for these measurements.

Figure 10 shows the experimental value of the dielectronic recombination rate coefficient, α_d, for hydrogenlike titanium, Ti XXII, as obtained from the spectrum in Fig. 4 by evaluation of the satellite to resonance line ratios. This value of α_d includes the contributions from the $n = 2$ satellites and from those $n = 3$ satellites which can be resolved on the wings of the apparent $Ly\alpha_1$ and $Ly\alpha_2$ line profiles. A part of the $n = 3$ satellites and all the $n \geq 4$ satellites are blended with the $Ly\alpha_1$ and the $Ly\alpha_2$ lines, and their contribution cannot be directly measured. However, since the theoretical results for the $n = 2$ satellites and the $n = 3$ satellites on the wings of the resonance lines are in very good agreement with the observation, we may assume that the predictions for the unresolved $n \geq 3$ satellites are also reliable. With this assumption we can obtain an estimate for the contribution from unresolved satellites to α_d. It is found to be of the order of the experimental error for α_d. The error bars shown in Fig. 10 mainly result from the experimental error of the laser Thomson scattering data which have been used for determining the electron temperature.

Also shown in Fig. 10 are predictions for the dielectronic recombination rate coefficient of Ti XXII from the detailed calculations of Safronova and Vainshtein and from the formulas of Burgess[39] and Merts et al.[40] The curve which represents Vainshtein and Safronova's results has been calculated from the line parameters given in Tables I and IIa – IVa. For this purpose the relative

intensity contribution, $I_s^{(n)}/I_R$, from satellites of the different n – shells was evaluated with use of Eq. (1) and the sum of these contributions was then multiplied by the values of the excitation rate coefficients, $C_R(T_e)$, given in reference.[1] This coefficient can be written in the form:

$$C_R(T_e) = \frac{6.828 \times 10^{-12}}{T_e^{1/2}} \exp\left(\frac{-E_0}{T_e}\right) \frac{1 + E_0/T_e}{0.24 + E_0/T_e} \tag{3}$$

where T_e is given in keV. Similarly, the experimental value for α_d was obtained by multiplying the observed total relative intensity $\Sigma_s I_s/I_R$, by $C_R(T_e)$. The experimental result is in very good agreement with both the predictions of Safronova and Vainshtein and Burgess' general formula.

VI. CONCLUSION

Dielectronic satellite spectra of hydrogenlike titanium, Ti XXII, have been observed from PLT tokamak plasmas and have been used for a detailed comparison with the theoretical results obtained by the Z – expansion method (Safronova and Vainshtein) and from Hartree – Fock calculations (Dubau et al.). The results due to the Z – expansion method are in excellent agreement with the experimental data except for minor discrepancies between theoretical and experimental wavelengths of 0.0003 Å for the $n = 2$ satellites and 0.0001 Å for the separation of the $Ly\alpha_1$ and $Ly\alpha_2$ lines. Very good agreement with the experimental data is also obtained for the results from the Hartree – Fock calculations although the discrepancies between the theoretical and experimental wavelengths $\simeq$ 0.0009Å for the $n = 2$ satellites are slightly larger.

The experimental data have also been used to determine the central ion and electron temperature of PLT discharges and to measure the dielectronic recombination rate coefficient, α_d, of Ti XXII. The experimental value for α_d is in good agreement with both the predictions from the detailed calculations by Safronova and Vainshtein[2] and from Burgess' general formula.[39]

ACKNOWLEDGMENTS:

The continued support of Dr. H.P. Furth, Dr. D.M. Meade, Dr. P.H. Rutherford, and Dr. J.C. Hosea is gratefully acknowledged. We deeply appreciate the discussions with Dr. J.P. Briand, Dr. R. Marrus, Dr. E. Hinnov, and Dr. S. Suckewer, and we also gratefully acknowledge the technical assistance of S. Winje, J. Gorman, J. Lehner, W. Urstadt, and the PLT technician crew under W. Mycock and assistance of the data processing group under R. Lusen. This work was supported by U.S. Department of Energy Contract No. DE-AC02-76-CHO-3073.

THIS PAGE

WAS INTENTIONALLY

LEFT BLANK

References

1 U.I. Safronova, A.M. Urnov, and L.A. Vainshtein, in the Proceedings of the P.N. Lebedev Physical Institute of the USSR Academy of Sciences, Moscow USSR, **119**, 13 (1980).

2 U.I. Safronova, (present calculations,1983).

3 J. Dubau, A.H. Gabriel, M. Loulergue, L. Steenman – Clark, and S. Volonte, Mon. Not. R. astr. Soc. **195**, 705 (1981).

4 J. Dubau, and L. Steenman–Clark, (present calculations, 1983).

5 G.W. Erickson, J. Phys. Chem. Ref. Data **6**, 831 (1977).

6 Y.I. Grineva, V.I. Karov, V.V. Korneev,V.V. Krutov, S.L. Mandelstam, L.A. Vainshtein, B.N. Vasilysev, and J.A. Zhitnik, Sol. Phys. **29**,441 (1973).

7 A.H. Gabriel, J.L. Culhane, L.W. Acton, E. Antonucci, R.D. Bentley, C. Jordan, L.W. Leibacher, A.N. Parmar, K.J.H. Phillips, C.G. Rapley, C.J. Wolfson, and K.T.Strong, Adv. Space Res. **1**, 267 (1981).

8 M. Bitter, K.W. Hill, N.R. Sauthoff, P.C. Efthimion, E. Meservey, W. Roney, S. von Goeler, R. Horton, M. Goldman, and W. Stodiek, Phys. Rev. Lett. **43**, 129 (1979).

9 M. Bitter, S.von Goeler, K. W. Hill, R. Horton, D. Johnson, W. Roney, N. Sauthoff, E. Silver, and W. Stodiek, Phys. Rev. Lett., **47**, 921 (1981).

10 T.F.R. Group, J. Dubau, M. Loulergue, J. Phys. B **15**, 1007 (1982).

11 F. Bely - Dubau, P. Faucher, L. Steenman - Clark, M. Bitter, S. von Goeler, K. W. Hill, C. Camhy - Val, and J. Dubau, Phys. Rev. A **26**, 3459 (1982).

12 R. Marrus in Beam – Foil Spectroscopy, edited by S. Bashkin (Springer–Verlag, 1976), Vol I, p. 209.

13 J.P. Briand, M. Tavernier, P. Indelicato, R. Marrus, and H.Gould, Phys. Rev. Lett. **50**, 832 (1983).

14 P. Indelicato, J.P. Briand, M. Tavernier, R. Marrus, and H. Gould, Fourth Topical Conference of the American Physical Society on Atomic Processes in High Temperature Plasmas , Princeton, New Jersey, 1983.

15 C. Breton, C. De Michelis, M. Finkenthal,and M. Mattioli, Fontenay – aux – Roses Laboratory Report EUR – CEA – FC – 948, 1978 .

16 K. Brau, S. von Goeler, M. Bitter, R.D. Cowan, D. Eames, K. Hill, N. Sauthoff, E. Silver, and W. Stodiek, Phys. Rev. **22**, 2769 (1980).

17 M. Bitter, S. von Goeler, N. Sauthoff, K.W. Hill, K. Brau, D. Eames, M. Goldman, E. Silver, and W. Stodiek, in Inner – Shell and X – Ray

Physics of Atoms and Solids , (Plenum Press, New York, 1981), p. 861.

18 W. Stodiek et al., in Proceedings of the 8th International Conference on Plasma Physics and Nuclear Fusion Research, Brussels, 1980, Vol. I, p. 9.

19 S.M. Younger, Phys. Rev. A **22**, 111 (1980).

20 D. Manos, D. Ruzic, R. Moore, and S. Cohen, J. Vac. Sci. Technol.**20**, 1230 (1982).

21 R.A. Boie, J. Fischer, Y. Inagaki, F.C. Merritt, V. Radeka, L.C. Rogers, and D.M. Xi, Nucl. Instrum. Methods **201**, 93 (1982).

22 H. Johann, Z. Phys. **69**, 189 (1931).

23 R. Hawryluk et al., Phys. Rev. Lett. **49**, 326 (1982).

24 M. Bitter, S. von Goeler, M. Goldman, K.W. Hill, R. Horton, W. Roney, N. Sauthoff, and W. Stodiek, in Temperature, Its Measurement and Control in Science and Industry , edited by J.F. Schooley (American Institute of Physics, New York, 1982), Vol. 5, p. 693.

25 S. von Goeler, M. Bitter, S. Cohen, D. Eames, K.W. Hill, D. Hillis, R. Hulse, G. Lenner, D. Manos, P. Roney, W. Roney, N. Sauthoff, S. Sesnic, W. Stodiek, F. Tenney, and J. Timberlake, in Proceedings of the Course on Diagnostics for Fusion Reactor Conditions, Varenna/Italy, 1982, Vol. I, p. 109.

26 E. Källne, J. Källne, and J.E. Rice, Phys. Rev. Lett. **49**, 330 (1982).

27 G.A. Doschek, R.W. Kreplin, and U. Feldman, Āstrophys. J. **233**, L157 (1979).

28 I.L. Beigman, L.A. Bureeva, and I.Yu. Skobolev, Sov. Astron. **23(6)**, 725 (1979).

29 U.I. Safronova, J. Quant. Spectrosc. Radiat. Transfer **15**, 231 (1975).

30 J. Dubau, M. Loulergue, and L. Steenman – Clark, Mon. Not. R. astr. Soc. **190**, 125 (1980).

31 B.W. Shore, Astrophys. J. **158**, 1205 (1969).

32 F. Bely – Dubau, A.H. Gabriel, and S. Volonte, Mon. Not. R. astr. Soc. **189**, 801 (1979).

33 H.A. Bethe and E.E. Salpeter, Quantum Mechanics of One- and Two-Electron Atoms (Springer - Verlag, Berlin, 1957).

34 G. Breit and E. Teller, Astrophys. J. **91**, 215 (1940).

35 G.F.W. Drake, Phys. Rev. A **3**, 908 (1971).

36 R.A. Hulse, Nucl. Technol./Fusion **3**, 259 (1983).

37 B.N. Chichkov, M.A. Mazing, A.P. Shevelko, and A.M. Urnov, Phys. Lett. **83A**, 401 (1981).

38 F. Bely – Dubau, M. Bitter, J. Dubau, P. Faucher, A.H. Gabriel, K.W. Hill, S. von Goeler, N. Sauthoff, and S. Volonte, Phys. Lett. **93A**, 189 (1983).

39 A. Burgess, Astrophys. J. **141**, 1588 (1965).

40 A.L. Merts, R.D.Cowan, and N.H. Magee, Los Alamos Scientific Laboratory Report LA - 6220 - MS, 1976.

TABLE CAPTIONS

Table I — Experimental wavelengths and theoretical results of Safronova and Vainshtein (superscript a) and Dubau et al. (superscript b) for the $Ly\alpha_1$ and $Ly\alpha_2$ lines of Ti XXII and the n = 2 satellites. The wavelengths are in Å. The radiative probability A, the autoionization probability Γ, and the line factor Q_D are in 10^{13} sec^{-1}. The key letters agree with Safronova's notation.

Table IIa — Atomic data of Safronova and Vainshtein for satellite lines to the Ti XXII resonance line due to transitions $2\ell'3\ell - 1s3\ell$. The wavelengths are in Å. The radiative probability A, the autoionization probability Γ, and the line factors Q_D are in 10^{13} sec^{-1}.

Table IIb — Atomic data of Dubau et al. for satellite lines to the Ti XXII resonance line due to transitions $2\ell'3\ell - 1s3\ell$. The wavelengths are in Å. The radiative probability A, the autoionization probability Γ, and the line factors Q_D are in 10^{13} sec^{-1}.

Table IIIa — Atomic data of Safronova and Vainshtein for satellite lines to the Ti XXII resonance line due to transitions $2\ell'4\ell - 1s4\ell$. The wavelengths are in Å. The radiative probability A, the autoionization probability Γ, and the line factors Q_D are in 10^{13} sec^{-1}.

Table IIIb — Atomic data of Dubau et al. for satellite lines to the Ti XXII resonance line due to transitions $2\ell'4\ell - 1s4\ell$. The wavelengths are in Å. The radiative probability A, the autoionization probability Γ, and the line factors Q_D are in 10^{13} sec^{-1}.

Table IVa — Atomic data of Safronova and Vainshtein for satellite lines to the Ti XXII resonance line due to transitions $2\ell'5\ell - 1s5\ell$. The wavelengths are in Å. The radiative probability A, the autoionization probability Γ, and the line factors Q_D are in $10^{13}sec^{-1}$.

Table IVb — Atomic data of Dubau et al. for satellite lines to the Ti XXII resonance line due to transitions $2\ell5\ell - 1s5\ell$. The wavelengths are in Å. The radiative probability A, the autoionization probability Γ, and the line factors Q_D are in $10^{13}sec^{-1}$.

TABLE I

PEAK	KEY	TRANSITION	λ_{exp} (Å)	λ_{theor} (Å)	A	Γ	Q_D
1		$1s(^2S_{1/2}) - 2p(^2P_{3/2})$	2.4903	2.4904[a] 2.4903[b]	15.000[a] 14.450[b]	-	
	V	$1s2s(^3S_1) - 2s2p(^1P_1)$		2.4915[a] 2.4905[b]	0.246[a] 0.189[b]	20.000[a] 16.940[b]	0.424[a] 0.314[b]
2		$1s(^2S_{1/2}) - 2p(^2P_{1/2})$	2.4957*	2.4957[a] 2.4956[b]	14.900[a] 14.360[b]	-	-
	M	$1s2p(^1P_1) - 2p^2(^1S_o)$		2.4973[a] 2.4960[b]	24.300[a] 22.960[b]	3.000[a] 2.703[b]	2.670[a] 2.415[b]
	T	$1s2s(^1S_o) - 2s2p(^1P_1)$		2.5046[a] 2.5033[b]	14.500[a] 13.400[b]	20.000[a] 16.940[b]	25.000[a] 22.290[b]
3			2.5044				
	K	$1s2p(^3P_2) - 2p^2(^1D_2)$		2.5052[a] 2.5042[b]	3.930[a] 3.109[b]	30.600[a] 27.690[b]	10.100[a] 7.878[b]
4	Q	$1s2s(^3S_1) - 2s2p(^3P_2)$	2.5066	2.5070[a] 2.5066[b]	14.500[a] 13.670[b]	1.360[a] 1.286[b]	6.210[a] 5.877[b]
5	B	$1s2p(^3P_1) - 2p^2(^3P_2)$	2.5077	2.5081[a] 2.5070[b]	8.190[a] 7.570[b]	6.720[a] 5.012[b]	7.720[a] 5.890[b]
	R	$1s2s(^3S_1) - 2s2p(^3P_1)$		2.5108[a] 2.5101[b]	14.200[a] 13.480[b]	1.670[a] 1.521[b]	4.430[a] 4.049[b]
6	A	$1s2p(^3P_2) - 2p^2(^3P_2)$	2.5115	2.5116[a] 2.5106[b]	17.800[a] 17.330[b]	6.720[a] 5.012[b]	16.800[a] 13.400[b]
	S	$1s2s(^3S_1) - 2s2p(^3P_o)$		2.5122[a] 2.5115[b]	14.400[a] 13.670[b]	1.360[a] 1.290[b]	1.240[a] 1.186[b]
	F	$1s2p(^3P_1) - 2p^2(^3P_o)$		2.5126[a] 2.5113[b]	27.400[a] 26.120[b]	0.249[a] 0.167[b]	0.244[a] 0.1642[b]
7	J	$1s2p(^1P_1) - 2p^2(^1D_2)$	2.5130	2.5132[a] 2.5123[b]	25.100[a] 23.820[b]	30.600[a] 27.690[b]	64.40[a] 60.36[b]
8	G	$1s2p(^1P_1) - 2p^2(^3P_2)$	2.5195	2.5196[a] 2.5187[b]	2.970[a] 2.293[b]	6.720[a] 5.012[b]	2.800[a] 1.784[b]
	P	$1s2p(^3P_1) - 2s^2(^1S_o)$		2.5272[a] 2.5266[b]	1.370[a] 1.123[b]	32.900[a] 29.390[b]	1.180[a] 0.953[b]
	O	$1s2p(^1P_1) - 2s^2(^1S_o)$		2.5388[a] 2.5385[b]	4.130[a] 4.111[b]	32.900[a] 29.390[b]	3.540[a] 3.489[b]

*The experimental wavelengths are relative to the theoretical value of 2.4957 Å for the $1s(^2S_{1/2}) - 2P(^2P_{1/2})$ transition.

Table IIa

Transition	λ(Å)	A	Γ	Q_d
$2p3p(^1S_o) - 1s3p(^1P_1)$	2.4874	12.800	1.600	1.160
$2p3d(^1P_1) - 1s3p(^1D_2)$	2.4878	13.300	0.091	0.248
$2p3d(^1F_3) - 1s3d(^3D_2)$	2.4881	4.920	2.400	4.720
$2p3s(^1P_1) - 1s3s(^3S_1)$	2.4883	0.712	8.580	0.918
$2p3d(^1F_3) - 1s3d(^3D_3)$	2.4885	1.220	2.400	1.170
$2p3d(^1F_3) - 1s3d(^1D_2)$	2.4886	8.950	2.400	8.600
$2p3p(^1D_2) - 1s3p(^3P_1)$	2.4888	0.191	11.100	0.440
$2p3p(^1D_2) - 1s3p(^3P_3)$	2.4898	1.220	11.100	2.810
$2p3d(^3P_1) - 1s3d(^3D_1)$	2.4910	8.770	0.0627	0.114
$2p3s(^1P_1) - 1s3s(^1S_1)$	2.4917	8.240	8.580	10.600
$2p3p(^1D_2) - 1s3p(^1P_1)$	2.4919	8.940	11.100	20.600
$2p3d(^3D_3) - 1s3d(^3D_2)$	2.4928	6.260	0.163	0.472
$2p3d(^3D_3) - 1s3d(^3D_3)$	2.4932	8.090	0.163	0.610
$2p3s(^3P_2) - 1s3s(^3S_1)$	2.4938	11.900	0.133	0.526
$2p3d(^3D_2) - 1s3d(^3D_2)$	2.4939	5.470	0.0620	0.114
$2p3d(^3D_2) - 1s3d(^3D_1)$	2.4939	4.870	0.0620	1.010
$2s3d(^1D_2) - 1s3d(^3D_3)$	2.4943	3.640	0.0620	0.0757
$2p3p(^3D_3) - 1s3p(^3P_2)$	2.4945	4.580	3.0500	6.270
$2p3s(^1P_1) - 1s3d(^3D_1)$	2.4946	0.797	8.5800	1.030
$2p3p(^3D_3) - 1s3p(^3P_2)$	2.4947	10.300	0.176	0.968
$2p3s(^1P_1) - 1s3d(^1D_2)$	2.4951	0.263	8.580	0.340
$2p3d(^3F_4) - 1s3d(^3D_3)$	2.4953	15.000	0.533	4.640
$2p3d(^3D_1) - 1s3d(^3D_2)$	2.4963	8.380	0.542	0.898
$2p3d(^3D_1) - 1s3d(^3D_1)$	2.4963	5.120	0.542	0.549
$2s3d(^3D_1) - 1s3p(^3P_1)$	2.4964	1.380	0.201	0.146
$2p3s(^1D_2) - 1s3s(^3S_1)$	2.4964	8.660	0.502	1.120

Table IIa Con't.

Transition	λ (Å)	A	Γ	ϱ_D
$2p3p(^3P_1) - 1s3p(^3P_1)$	2.4966	13.70	0.246	0.191
$2s3d(^3D_2) - 1s3p(^3P_2)$	2.4974	2.210	2.410	3.230
$2s3d(^3D_1) - 1s3p(^3P_2)$	2.4974	2.810	0.201	0.297
$2p3d(^1D_2) - 1s3d(^1D_2)$	2.4975	9.430	0.0392	0.129
$2s3d(^1D_2) - 1s2p(^1P_1)$	2.4976	1.770	3.050	2.430
$2s3p(^3P_1) - 1s3s(^3S_1)$	2.4979	4.880	0.123	0.0710
$2p3d(^3F_3) - 1s3d(^3D_2)$	2.4985	3.820	0.576	0.9960
$2s3p(^3P_1) - 1s3s(^3S_1)$	2.4985	3.300	0.896	1.170
$2p3d(^3F_3) - 1s3d(^3D_3)$	2.4989	5.660	0.576	1.470
$2p3d(^3F_3) - 1s3d(^1D_2)$	2.4990	5.410	0.576	1.410
$2p3s(^3P_o) - 1s3s(^3S_1)$	2.4992	4.650	0.0732	0.403
$2p3s(^3P_o) - 1s3s(^3S_1)$	2.4993	9.780	0.5600	0.469
$2s3d(^3D_2) - 1s3p(^1P_1)$	2.4995	2.400	2.410	3.520
$2p3p(^3D_2) - 1s3p(^3P_1)$	2.5004	4.870	0.615	1.040
$2p3d(^3F_2) - 1s3d(^3D_2)$	2.5006	5.850	0.397	0.762
$2p3d(^3F_2) - 1s3d(^3D_1)$	2.5006	7.760	0.397	1.010
$2p3p(^3D_2) - 1s3p(^3P_2)$	2.5014	4.510	0.615	0.962
$2s3s(^1P_1) - 1s3p(^3P_1)$	2.5032	1.170	16.400	0.935
$2p3p(^3D_2) - 1s3p(^1P_1)$	2.5035	1.590	0.615	0.339
$2s3p(^3P_2) - 1s3d(^3D_3)$	2.5041	1.440	0.587	0.718
$2s3p(^1P_1) - 1s3s(^1P_1)$	2.5048	5.650	0.100	0.171
$2s3s(^1P_1) - 1s3p(^1P_1)$	2.5064	2.150	16.400	1.710
$2s3s(^3P_1) - 1s3p(^3P_2)$	2.5077	1.920	0.0736	0.107

Table IIIa

Transition	λ(Å)	A	Γ	Q_d
$2p4d(^1F_3) - 1s4d(^3D_2)$	2.4896	4.82	0.9000	1.9000
$2p4p(^1S_1) - 1s4p(^1P_1)$	2.4896	13.400	1.0700	0.8650
$2p4d(^1F_3) - 1s4d(^1D_3)$	2.4898	2.780	0.9000	1.1000
$2p4d(^1F_3) - 1s4d(^1D_2)$	2.4898	7.450	0.9000	2.9400
$2p4d(^1P_1) - 1s4d(^3S_1)$	2.4903	2.580	2.9000	1.4000
$2p4p(^1D_2) - 1s4p(^3P_2)$	2.4907	4.390	4.7200	4.9900
$2p4d(^3P_1) - 1s4d(^3D_1)$	2.4908	10.800	0.0265	0.0579
$2p4d(^3D_3) - 1s4d(^3D_2)$	2.4915	8.820	0.1150	0.4690
$2p4p(^1D_2) - 1s4p(^3P_1)$	2.4916	9.830	4.7200	11.2000
$2p4d(^3P_2) - 1s4s(^3S_1)$	2.4916	13.600	0.0457	0.2080
$2p4d(^3D_3) - 1s4d(^3D_3)$	2.4917	5.210	0.1150	0.2770
$2p4p(^3P_2) - 1s4p(^3P_1)$	2.4917	11.500	0.9880	3.2800
$2p4s(^1P_1) - 1s4s(^1S_1)$	2.4918	10.000	2.9000	5.4400
$2p4d(^1D_2) - 1s4d(^3D_2)$	2.4920	4.520	0.0413	0.0622
$2p4d(^1D_2) - 1s4d(^3D_1)$	2.4920	4.890	0.0413	0.0673
$2p4p(^3P_2) - 1s4p(^3P_2)$	2.4921	2.580	0.9880	0.7340
$2p4d(^1D_2) - 1s4d(^1D_2)$	2.4922	3.490	0.0413	0.0480
$2p4d(^3F_4) - 1s4d(^3D_3)$	2.4924	15.000	0.2250	2.0000
$2p4p(^3D_3) - 1s4p(^3P_2)$	2.4926	14.300	0.0354	0.2200
$2s4d(^1D_2) - 1s4p(^3P_1)$	2.4945	0.922	0.0330	0.0673
$2s4d(^1D_2) - 1s4p(^3P_2)$	2.4949	1.010	0.0330	0.0738
$2p4s(^3P_1) - 1s4s(^3S_1)$	2.4953	6.890	1.1400	2.5000

Table IIIa Con't.

Transition	λ (Å)	A	Γ	Q_d
$2p4p(^3P_o) - 1s4p(^3P_1)$	2.4957	12.600	0.1370	0.1200
$2s4d(^3D_1) - 1s4p(^3P_1)$	2.4960	1.110	0.0889	0.0659
$2s4d(^3D_2) - 1s4p(^3P_2)$	2.4964	1.860	0.0707	1.3300
$2s4d(^3D_1) - 1s4p(^3P_2)$	2.4964	2.460	0.0889	0.1460
$2p4d(^3D_2) - 1s4d(^3D_3)$	2.4964	8.290	0.0193	0.0578
$2p4d(^3F_3) - 1s4d(^3D_2)$	2.4965	1.380	0.3100	0.1970
$2p4d(^3F_3) - 1s4d(^3D_3)$	2.4967	6.980	0.3100	0.9930
$2p4d(^3F_3) - 1s4d(^1D_2)$	2.4967	6.560	0.3100	0.9330
$2s4p(^3P_1) - 1s4s(^3S_1)$	2.4967	1.240	0.4070	0.3830
$2s4d(^3D_3) - 1s4p(^3P_2)$	2.4968	0.675	0.0697	0.3970
$2p4s(^3P_o) - 1s4s(^3S_1)$	2.4972	10.200	0.2280	0.2110
$2s4d(^3D_2) - 1s4p(^1P_1)$	2.4973	1.770	0.7070	1.2600
$2p4p(^3D_2) - 1s4p(^3P_1)$	2.4974	2.380	0.7990	0.7610
$2p4d(^3F_2) - 1s4d(^3D_2)$	2.4977	6.630	0.1770	0.3920
$2p4d(^3F_2) - 1s4d(^3D_1)$	2.4977	8.020	0.1770	0.4750
$2p4p(^3D_2) - 1s4p(^3P_2)$	2.4978	5.130	0.7990	1.6400
$2s4p(^1P_1) - 1s4s(^3S_1)$	2.4979	4.030	0.0643	0.7920
$2p4p(^3P_1) - 1s4p(^1P_1)$	2.4979	4.470	0.0112	0.0120
$2p4p(^3D_2) - 1s4p(^1P_1)$	2.4987	2.890	0.7990	0.9220
$2p4p(^1S_1) - 1s4p(^3P_1)$	2.4987	1.940	6.4900	1.2100
$2s4p(^3P_2) - 1s4d(^3D_3)$	2.4991	1.490	0.2250	0.4480
$2s4p(^1P_1) - 1s4s(^1S_1)$	2.4993	4.510	0.0643	0.0887
$2s4p(^3P_1) - 1s4d(^3D_2)$	2.4994	0.564	0.4070	0.1740
$2s4s(^1S_1) - 1s4p(^1P_1)$	2.5001	1.560	6.4900	0.9710
$2s4s(^3S_1) - 1s4p(^3P_2)$	2.5005	1.790	0.0281	0.0492

Table IVa

Transition	λ (Å)	A	Γ	Q_d
$2p5d(^1F_2) - 1s5d(^3D_2)$	2.4900	4.600	0.419	0.873
$2p5d(^1F_3) - 1s5d(^3D_3)$	2.4901	3.910	0.419	0.741
$2p5d(^1F_3) - 1s5d(^1D_2)$	2.4901	6.540	0.419	1.240
$2p5p(^1S_0) - 1s5p(^1P_1)$	2.4902	13.500	0.746	0.6170
$2p5s(^1P_1) - 1s5s(^3S_1)$	2.4906	3.930	1.070	0.8150
$2p5p(^1D_2) - 1s5p(^3P_2)$	2.4906	5.860	2.120	3.4500
$2p5d(^3D_3) - 1s5d(^3D_2)$	2.4910	9.850	0.693	0.3160
$2p5s(^3P_2) - 1s5s(^3S_1)$	2.4910	14.500	0.0294	0.1420
$2p5p(^1D_2) - 1s5p(^1P_1)$	2.4911	9.030	2.1200	5.3100
$2p5d(^3D_3) - 1s5d(^3D_3)$	2.4911	4.010	0.0693	0.1290
$2p5p(^3P_2) - 1s5p(^3P_1)$	2.4911	13.000	0.6400	2.5100
$2p5s(^1P_1) - 1s5s(^1S_1)$	2.4913	10.200	1.0700	2.1100
$2p5p(^3P_2) - 1s5p(^3P_2)$	2.4913	1.240	0.6400	0.2380
$2p5d(^3F_4) - 1s5d(^3D_3)$	2.4914	15.000	0.1150	1.0300
$2p5p(^3D_3) - 1s5p(^3P_2)$	2.4916	14.900	0.0124	0.0814
$2s5d(^1D_2) - 1s5p(^3P_1)$	2.4950	0.333	0.0449	0.0499
$2s5d(^1D_2) - 1s5p(^3P_2)$	2.4952	0.918	0.0449	0.1370
$2s5p(^1P_1) - 1s5s(^3S_1)$	2.4953	5.000	0.9790	1.9900
$2p5p(^3P_o) - 1s5p(^3P_1)$	2.4955	11.300	0.0634	0.0572
$2s5p(^1P_1) - 1s5s(^1S_1)$	2.4960	0.560	0.9790	0.2230
$2s5d(^3D_2) - 1s5p(^3P_2)$	2.4960	1.780	0.3240	0.6930
$2s5d(^3D_1) - 1s5p(^3P_2)$	2.4960	2.440	0.0457	0.0799
$2p5d(^3F_3) - 1s5d(^3D_3)$	2.4961	7.080	0.189	0.6200

Table IVa Con't.

Transition	λ(Å)	A	Γ	Q_d
$2p5d(^3F_3) - 155d(^1D_2)$	2.4961	7.270	0.1890	0.6370
$2s5d(^3D_3) - 1s5p(^3P_2)$	2.4962	0.138	0.0414	0.2120
$2s5p(^3P_1) - 1s5s(^3S_1)$	2.4962	0.657	0.2150	0.1720
$2p5s(^3P_o) - 1s5s(^3S_1)$	2.4965	10.500	0.1140	0.1100
$2s5d(^3D_2) - 1s5p(^1P_1)$	2.4965	1.610	0.3240	0.6260
$2p5p(^3D_2) - 1s5p(^3P_1)$	2.4965	1.490	0.5790	0.3740
$2p5d(^3F_2) - 1s5d(^3D_2)$	2.4967	6.930	0.0899	0.2090
$2p5d(^3F_2) - 1s5d(^3D_1)$	2.4967	7.720	0.0899	0.2330
$2p5p(^3D_2) - 1s5p(^3P_2)$	2.4967	5.180	0.5790	1.3000
$2p5s(^3P_1) - 1s5s(^3S_1)$	2.4968	5.220	0.0374	0.0586
$2p5p(^3D_2) - 1s5p(^1P_1)$	2.4972	3.560	0.5790	0.8950
$2p5p(^1S_1) - 1s5p(^3P_1)$	2.4972	2.590	3.1400	1.1300
$2s5p(^3P_2) - 1s5d(^3D_3)$	2.4974	1.450	0.1100	0.2750
$2s5p(^3P_1) - 1s5d(^3D_2)$	2.4975	0.5570	0.2150	0.1460
$2p5p(^1S_1) - 1s5p(^1P_1)$	2.4979	1.1900	3.1400	0.5190

Table IIb

Transition	λ (Å)	A	T	Ω_D
$2s3p(^1P_1) - 1s3s(^1S_0)$	2.5033	0.1083	4.9540	0.1718
$2s3s(^1S_0) - 1s3p(^3P_1)$	2.5028	13.1800	0.8177	0.6474
$2s3s(^1S_0) - 1s3p(^1P_1)$	2.5060	13.1800	2.0390	1.6140
$2s3p(^3P_0) - 1s3s(^3S_1)$	2.4985	0.5176	6.9600	0.4103
$2s3p(^3P_1) - 1s3s(^3S_1)$	2.4978	0.7045	3.0080	0.9619
$2s3p(^3P_1) - 1s3d(^3D_2)$	2.5034	0.5869	0.4969	0.1610
$2s3p(^3P_2) - 1s3d(^3D_3)$	2.5030	0.4823	1.2980	0.5921
$2p3p(^3D_2) - 1s3p(^3P_1)$	2.4991	0.4144	3.8820	0.6380
$2p3p(^3D_2) - 1s3p(^3P_2)$	2.5002	0.4144	3.4800	0.5720
$2p3s(^3P_1) - 1s3s(^3S_1)$	2.4953	0.3737	8.3670	0.8315
$2s3d(^3D_3) - 1s3p(^3P_2)$	2.4985	0.0617	3.6140	0.2420
$2p3d(^3F_2) - 1s3s(^3S_1)$	2.4925	0.2621	3.1980	0.3093
$2p3d(^3F_2) - 1s3d(^3D_1)$	2.4991	0.2046	4.0350	0.2936
$2p3d(^3F_2) - 1s3d(^3D_2)$	2.4991	0.2046	1.9050	0.1386
$2p3s(^3P_2) - 1s3s(^3S_1)$	2.4931	0.1941	5.4160	0.3713
$2p3s(^3P_2) - 1s3d(^3D_1)$	2.4993	0.1941	3.8200	0.2619
$2s3d(^3D_1) - 1s3p(^3P_2)$	2.4962	0.1719	2.0420	0.1630
$2s3d(^3D_2) - 1s3p(^3P_1)$	2.4951	1.8030	0.3635	0.4189
$2s3d(^3D_2) - 1s3p(^3P_2)$	2.4965	2.7450	2.3130	3.2460
$2s3d(^3D_2) - 1s3p(^1P_1)$	2.4986	2.7460	3.0520	4.2840
$2p3d(^3F_3) - 1s3d(^3D_2)$	2.4973	0.4406	3.9650	0.8557
$2p3d(^3F_3) - 1s3d(^3D_3)$	2.4977	0.4406	4.8960	1.0570
$2p3d(^3F_2) - 1s3d(^1D_2)$	2.4973	0.4282	4.4510	0.9693
$2s3d(^1D_2) - 1s3p(^3P_1)$	2.4938	1.8040	2.4938	3.6560
$2s3d(^1D_2) - 1s3p(^3P_2)$	2.4948	1.8040	0.6675	0.6972

Table IIb Con't.

Transition	λ(Å)	A	T	Q_D
$2s3d(^1D_2) - 1s3p(^1P_1)$	2.4969	1.8040	1.0580	1.1050
$2p3d(^1D_2) - 1s3d(^1D_2)$	2.4960	0.0457	8.9270	0.1494
$2p3p(^3D_3) - 1s3p(^3P_2)$	2.4936	0.1419	9.7490	0.7779
$2p3d(^3D_1) - 1s3s(^1S_0)$	2.4913	0.7606	1.0580	0.1579
$2p3d(^3D_1) - 1s3d(^3D_1)$	2.4950	0.9329	4.4360	0.7848
$2p3d(^3D_1) - 1s3d(^3D_2)$	2.4950	0.9329	7.2030	1.2770
$2p3d(^3F_4) - 1s3d(^3D_3)$	2.4945	0.4146	13.5500	3.6200
$2p3p(^3P_2) - 1s3p(^3P_1)$	2.4918	0.0355	5.9400	0.0672
$2p3p(^3P_2) - 1s3p(^3P_2)$	2.4929	0.0355	6.3630	0.07198
$2p3s(^1P_1) - 1s3s(^3S_1)$	2.4875	6.2480	0.5975	0.6468
$2p3s(^1P_1) - 1s3s(^1S_0)$	2.4907	6.2480	7.2050	7.8000
$2p3s(^1P_1) - 1s3d(^3D_1)$	2.4937	6.2480	1.1990	1.2980
$2p3s(^1P_1) - 1s3d(^3D_2)$	2.4938	6.2480	0.3642	0.3946
$2p3s(^1P_1) - 1s3d(^1D_2)$	2.4943	6.2480	0.2673	0.2894
$2p3d(^3D_3) - 1s3d(^3D_2)$	2.4918	0.1065	5.2780	0.2517
$2p3d(^3D_3) - 1s3d(^3D_3)$	2.4922	0.1065	7.8980	.37660
$2p3p(^1D_2) - 1s3p(^3P_1)$	2.4880	8.7190	0.2186	0.4385
$2p3p(^1D_2) - 1s3p(^3P_2)$	2.4880	8.7190	1.0340	2.0740
$2p3p(^1D_2) - 1s3p(^1P_1)$	2.5006	8.0440	0.0210	0.3664
$2p3d(^1F_3) - 1s3d(^3D_2)$	2.4870	1.8610	4.3760	3.1490
$2p3d(^1F_3) - 1s3d(^3D_3)$	2.4874	1.8610	0.9132	0.6571
$2p3d(^1F_3) - 1s3d(^1D_2)$	2.4875	1.8610	8.4300	6.0660
$2p3d(^1P_1) - 1s3d(^1D_2)$	2.4858	0.0799	11.3000	0.1908
$2p3p(^1S_0) - 1s3p(^1P_1)$	2.4866	1.3820	12.2900	1.0007

Table IIIb

Transition	λ(Å)	A	Γ	Q_D
$2s4s(^1S_0) - 1s4p(^3P_1)$	2.4978	4.669	0.8188	0.5410
$2s4s(^1S_0) - 1s4p(^1P_1)$	2.4991	4.669	1.348	0.8907
$2s4p(^1P_1) - 1s4s(^3S_1)$	2.4962	0.1948	1.862	0.1596
$2s4p(^1P_1) - 1s4s(^1S_0)$	2.4975	0.1948	3.297	0.2826
$2s4p(^3P_0) - 1s4s(^3S_1)$	2.4959	0.2145	3.328	0.1543
$2s4p(^3P_1) - 1s4s(^3S_1)$	2.4956	0.2851	1.092	0.3103
$2s4p(^3P_1) - 1s4d(^3D_2)$	2.4982	0.2851	0.4815	0.1368
$2s4p(^3P_2) - 1s4d(^3D_3)$	2.4980	0.1955	0.9869	0.3638
$2s4d(^3D_2) - 1s4p(^3P_2)$	2.4958	0.2518	1.214	0.2702
$2s4d(^3D_2) - 1s4p(^3P_2)$	2.4962	0.2518	1.976	0.4398
$2s4d(^3D_2) - 1s4p(^1P_1)$	2.4971	0.2518	1.059	0.2357
$2s4d(^3D_3) - 1s4p(^3P_2)$	2.4958	0.0616	0.5294	0.1465
$2p4s(^3P_1) - 1s4s(^3S_1)$	2.4935	0.8090	7.774	1.882
$2p4s(^3P_1) - 1s4s(^1S_0)$	2.4948	0.8090	0.5515	0.1340
$2s4d(^1D_2) - 1s4p(^3P_2)$	2.4951	0.7034	1.322	0.9107
$2s4d(^1D_2) - 1s4p(^1P_1)$	2.4960	0.7034	2.305	1.588
$2p4d(^3F_2) - 1s4d(^3D_1)$	2.4957	0.0993	5.014	0.2679
$2p4d(^3F_2) - 1s4d(^3D_2)$	2.4957	0.0993	3.854	0.2059
$2s4f(^3F_3) - 1s4d(^3D_3)$	2.4953	0.0611	1.430	0.1587
$2s4f(^3F_3) - 1s4d(^1D_2)$	2.4954	0.0611	1.470	0.1632
$2p4p(^3D_2) - 1s4p(^3P_1)$	2.4935	0.2150	1.463	0.2175
$2p4p(^3D_2) - 1s4p(^3P_2)$	2.4940	0.2150	3.906	0.5806
$2p4p(^3D_2) - 1s4p(^1P_1)$	2.4948	0.2150	0.7108	0.1057
$2p4d(^3F_3) - 1s4d(^3D_2)$	2.4940	0.2278	0.6853	0.1059

Table IIIb Con't.

Transition	λ(Å)	A	Γ	Q_D
$2p4d(^3F_3) - 1s4d(^3D_3)$	2.4942	0.2278	4.951	0.7654
$2p4d(^3F_3) - 1s4d(^1D_4)$	2.4943	0.2278	4.044	0.6252
$2p4s(^1P_1) - 1s4s(^3S_1)$	2.4889	1.973	2.400	1.027
$2p4s(^1P_1) - 1s4s(^1S_0)$	2.4903	1.973	8.955	3.831
$2p4s(^1P_1) - 1s4d(^3D_1)$	2.4915	1.973	0.2426	0.1038
$2p4p(^3D_3) - 1s4p(^3P_2)$	2.4908	0.0432	12.68	0.2729
$2p4p(^3P_2) - 1s4p(^3P_1)$	2.4901	0.5371	10.35	1.872
$2p4p(^3P_2) - 2s4p(^3P_2)$	2.4905	0.5371	2.314	0.4185
$2p4d(^3F_4) - 1s4d(^3D_3)$	2.4906	0.1988	12.90	1.742
$2p4d(^3D_3) - 1s4d(^3D_2)$	2.4900	0.0954	7.851	0.3789
$2p4d(^3D_3) - 1s4d(^3D_3)$	2.4902	0.0954	4.435	0.2141
$2p4d(^1D_2) - 1s4p(^3P_2)$	2.4893	3.367	3.618	3.514
$2p4p(^1D_2) - 1s4p(^1P_1)$	2.4901	3.367	8.566	8.319
$2p4p(^1D_2) - 1s4f(^3F_2)$	2.4902	3.367	0.1042	0.1012
$2p4p(^1D_2) - 1s4f(^1F_3)$	2.4903	3.367	0.1748	0.1698
$2p4f(^1D_2) - 1s4f(^3F_2)$	2.4890	0.0404	8.805	0.1306
$2p4f(^3G_5) - 1s4f(^3F_4)$	2.4891	0.0237	13.15	0.2552
$2p4f(^1G_4) - 1s4f(^3F_3)$	2.4888	0.0362	10.10	0.2444
$2p4d(^1F_3) - 1s4d(^3D_2)$	2.4885	0.8364	4.027	1.578
$2p4d(^1F_3) - 1s4d(^3D_3)$	2.4886	0.8364	2.388	0.9360
$2p4d(^1F_3) - 1s4d(^1D_2)$	2.4887	0.8364	6.756	2.648
$2p4f(^3D_2) - 1s4f(^1F_3)$	2.4885	0.0535	13.03	0.2556
$2p4p(^1S_0) - 1s4p(^1P_1)$	2.4883	0.8409	11.94	0.6868

Table IVb

Transition	λ(Å)	A	Γ	Q_D
$2s5s(^1S_0) - 1s5p(^3P_1)$	2.4962	1.991	0.7090	0.3953
$2s5s(^1S_0) - 1s5p(^1P_1)$	2.4969	1.991	0.7913	0.4412
$2s5p(^1P_1) - 1s5s(^3S_1)$	2.4952	0.2172	1.649	0.2332
$2s5p(^1P_1) - 1s5s(^1S_0)$	2.4958	0.2172	1.929	0.2728
$2s5p(^3P_1) - 1s5s(^3S_1)$	2.4951	0.1436	0.4330	0.1339
$2s5p(^3P_1) - 1s5d(^3D_2)$	2.4964	0.1436	0.3536	0.1094
$2s5p(^3P_2) - 1s5d(^3D_3)$	2.4963	0.0879	0.6278	0.2077
$2s5d(^3D_2) - 1s5p(^3P_2)$	2.4954	0.0732	0.6929	0.1307
$2s5d(^1D_2) - 1s5p(^3P_2)$	2.4949	0.1236	0.6526	0.1779
$2s5d(^1D_2) - 1s5p(^1P_1)$	2.4953	0.1236	0.1154	0.3145
$2p5s(^3P_1) - 1s5s(^3S_1)$	2.4936	0.5585	7.406	1.205
$2p5s(^3P_1) - 1s5s(^1S_0)$	2.4942	0.5585	2.071	0.3370
$2p5d(^3F_2) - 1s5d(^3D_1)$	2.4943	0.0681	5.403	0.1664
$2p5d(^3F_2) - 1s5d(^3D_2)$	2.4943	0.0681	5.238	0.1613
$2p5p(^3D_2) - 1s5p(^3P_1)$	2.4937	0.4963	1.192	0.2679
$2p5p(^3D_2) - 1s5p(^3P_2)$	2.4939	0.4963	5.624	1.264
$2p5p(^3D_2) - 1s5p(^1P_1)$	2.4943	0.4963	3.176	0.7139
$2p5d(^3F_3) - 1s5d(^3D_3)$	2.4939	0.1872	6.030	0.6134
$2p5d(^3F_3) - 1s5d(^1D_2)$	2.4939	0.1872	5.925	0.6028
$2p5s(^1P_1) - 1s5s(^3S_1)$	2.4892	0.6843	3.665	0.5553
$2p5s(^1P_1) - 1s5s(^1S_0)$	2.4898	0.6843	9.022	1.367
$2p5p(^3D_3) - 1s5p(^3P_2)$	2.4898	0.0180	13.11	0.1204

Table IVb Con't.

Transition	λ(Å)	A	Γ	Q_D
$2p5p(^3P_2) - 1s5p(^3P_1)$	2.4896	0.3138	11.60	1.297
$2p5p(^3P_2) - 1s5p(^3P_2)$	2.4898	0.3138	1.175	0.1314
$2p5d(^3F_4) - 1s5d(^3D_3)$	2.4898	0.1042	13.11	0.9236
$2p5p(^1D_2) - 1s5p(^3P_2)$	2.4892	1.419	04.986	2.347
$2p5p(^1D_2) - 1s5p(^1P_1)$	2.4897	1.419	7.794	3.669
$2p5d(^3D_3) - 1s5d(^3D_2)$	2.4895	0.0578	8.720	0.2612
$2p5d(^3D_3) - 1s5d(^3D_3)$	2.4896	0.0578	3.520	0.1054
$2p5f(^3G_5) - 1s5f(^3F_4)$	2.4891	0.0184	13.18	0.1996
$2p5d(^1F_3) - 1s5d(^3D_2)$	2.4888	0.4216	3.866	0.8132
$2p5d(^1F_3) - 1s5d(^3D_3)$	2.4889	0.4216	3.390	0.7130
$2p5d(^1F_3) - 1s5d(^1D_2)$	2.4889	0.4216	5.938	1.249
$2p5p(^1S_0) - 1s5p(^1P_1)$	2.4889	0.5322	11.98	0.4499
$2p5f(^1G_4) - 1s5f(^3F_3)$	2.4889	0.0279	09.631	0.1814
$2p5f(^1D_2) - 1s5f(^1F_3)$	2.4888	0.0263	13.09	0.1279

FIGURE CAPTIONS

FIG. 1 Fractional abundance of the different states of ionization of titanium for coronal equilibrium as a function of the electron temperature (courtesy of Breton et al.)

FIG. 2 Satellite spectra of Ti XXII. The data have been accumulated from 17 PLT discharges with additional ion cyclotron heating of 4 MW during consecutive time intervals from 600-650 msec (Fig. 2a) and 650-700 msec (Fig. 2b). Approximately an amount of 1.5×10^{17} titanium atoms was injected into each discharge at the time of 650 msec.

FIG. 3 Typical electron density and electron temperature profiles of PLT discharges with 4 MW ion cyclotron heating as obtained from laser Thomson scattering.

FIG. 4 Satellite spectrum of Ti XXII accumulated from 78 almost identical rf heated PLT discharges with typical parameters shown in Fig. 3.

FIG. 5 Spectra of hydrogenlike oxygen, O VIII, magnesium, Mg XII, sulphur, SXVI, and calcium, Ca XX, from the PLT and ALCATOR tokamaks and from a solar flare, respectively. The spectra illustrate the Z-dependence of the doublet splitting of the $Ly\alpha_1$ and $Ly\alpha_2$ lines and of the dielectronic satellites.

FIG. 6 Experimental Ti XXII data and theoretical predictions (solid lines) of Dubau et al. (Fig. 6a) and Safronova and Vainshtein (Fig. 6b). Curve II - V and curve I represent the contributions from di-electronic satellites with n = 2-5, and the total intensity, respectively, including the contributions from the $Ly\alpha_1$ and $Ly\alpha_2$ lines (features 1 and 2). Also, included in the theoretical spectra is the contribution from the $2S_{1/2} - 1S_{1/2}$ magnetic dipole transition. Subfigure 6c shows the experimental data and the theoretical spectrum obtained from the results of Safronova and Vainshtein after a slight correction of the theoretical wavelengths of all the n = 2 satellites by the same amount of 0.0003 Å and with a value of 2.4903 Å (instead of Safronova's value of 2.4904 Å) for the wavelength of the $Ly\alpha_1$ line.

FIG. 7 Spectral range of the Lyα_1 and Lyα_2 lines and associated $n \geq 3$ satellites from Figs. 6b and 6c on an enlarged scale.

FIG. 8 Satellite to resonance line ratio, I_J/I_R, as observed from the spectrum in Fig. 4 versus the experimental value of the central electron temperature, and the predicted electron temperature dependence (solid line) from Eq. (1).

FIG. 9 Observed (apparent) Lyα_2 line profiles from the spectra in Figs. 2a and 2b with least squares fits of a single Voigt functions (solid lines). The arrows indicate the range used for the fit. The obtained ion temperature values are T_i = 2.0 $\pm$ 0.2 keV (for Fig. 9a) and T_i = 1.8 $\pm$ 0.1 keV (for Fig. 9b).

FIG. 10 Experimental value and theoretical predictions by Safrona and Vainshtein, Burgess, and Merts et al. for the dielectronic recombination rate coefficient, α_d, of T_i XXII. The error bars mainly result from the experimental error of the laser Thomson scattering data.

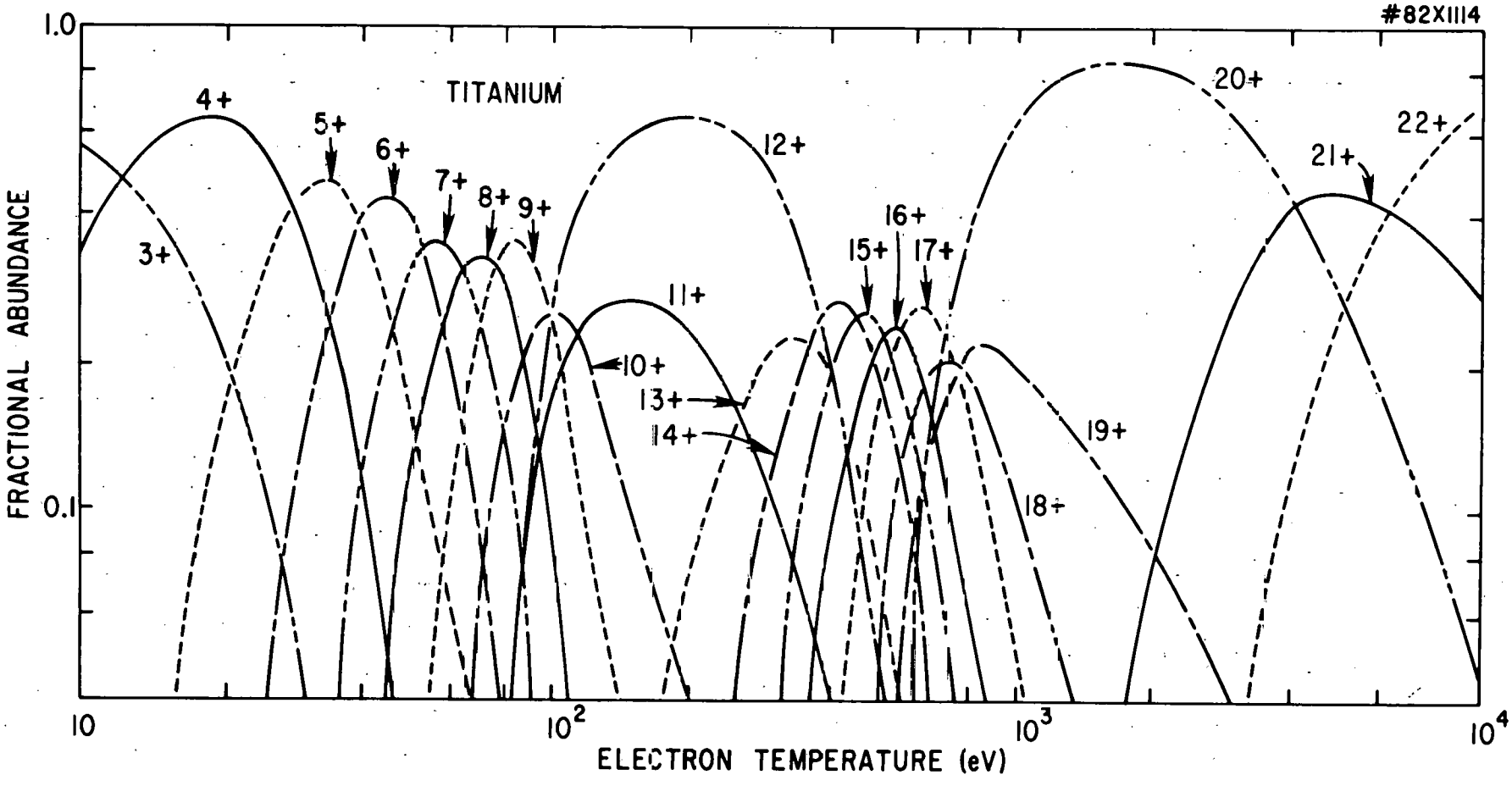
#82X1114
TITANIUM
1.0
0.1
FRACTIONAL ABUNDANCE
10
10^2
10^3
10^4
ELECTRON TEMPERATURE (eV)
3+
4+
5+
6+
7+
8+
9+
10+
11+
12+
13+
14+
15+
16+
17+
18+
19+
20+
21+
22+

Fig. 1

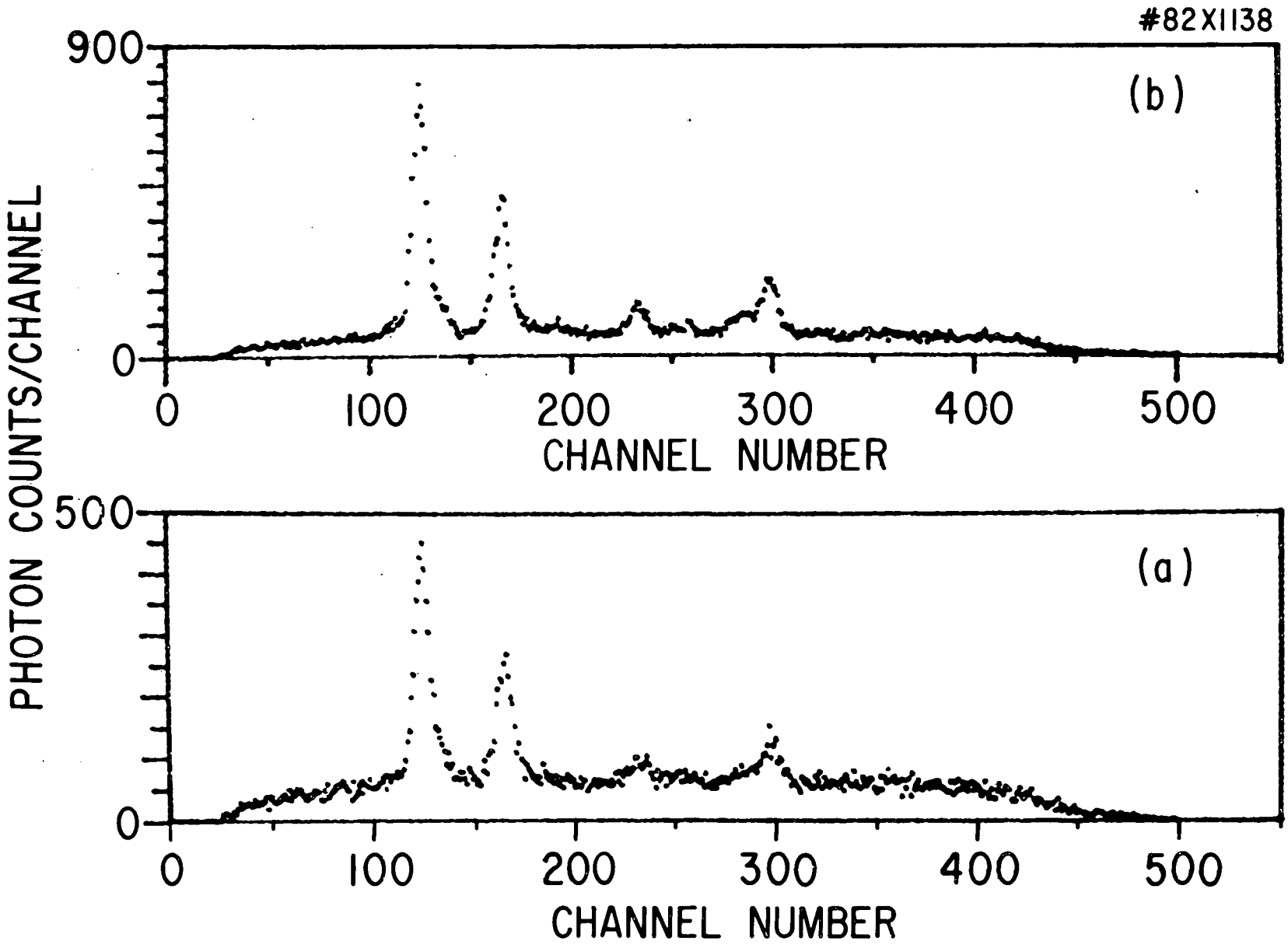
#82X1138
900
0
(b)
0
100
200
300
400
500
CHANNEL NUMBER
PHOTON COUNTS/CHANNEL
500
0
(a)
0
100
200
300
400
500
CHANNEL NUMBER

Fig. 2

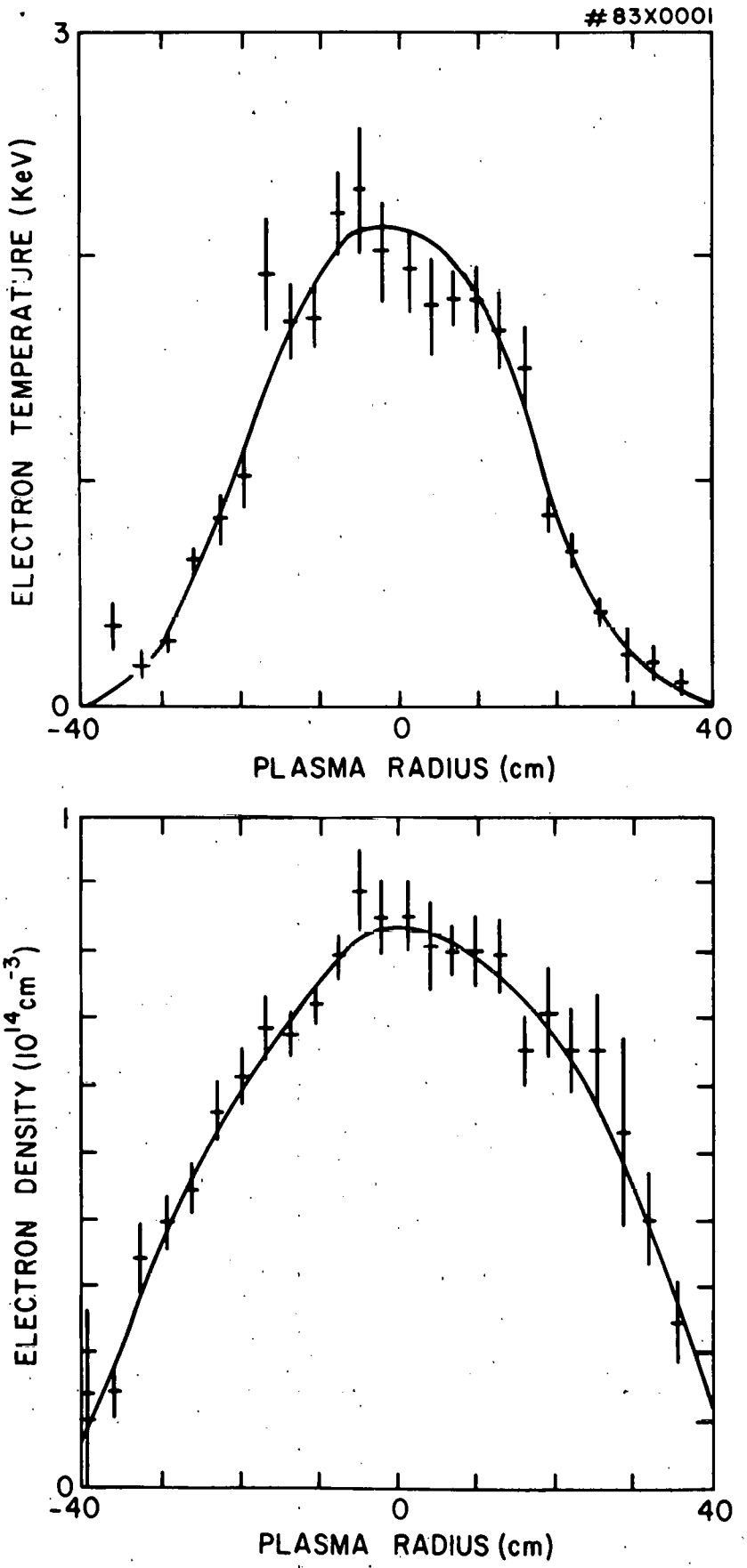
#83X0001
3
0
ELECTRON TEMPERATURE (KeV)
-40
0
40
PLASMA RADIUS (cm)
1
0
ELECTRON DENSITY ($10^{14}cm^{-3}$)
-40
0
40
PLASMA RADIUS (cm)

Fig. 3

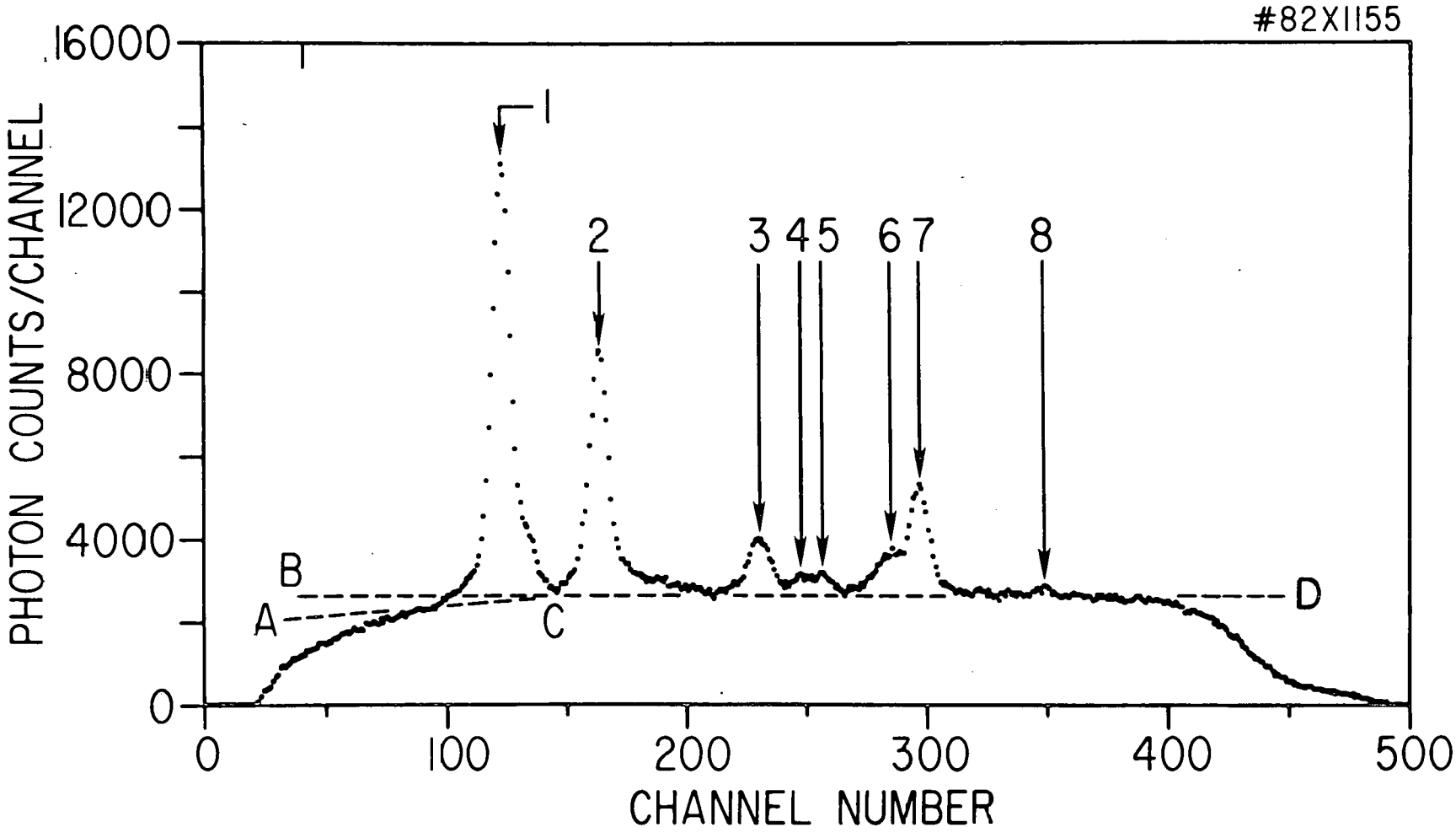
#82X1155
16000
12000
8000
4000
0
PHOTON COUNTS/CHANNEL
1
2
3 4 5
6 7
8
A
B
C
D
0
100
200
300
400
500
CHANNEL NUMBER

Fig. 4

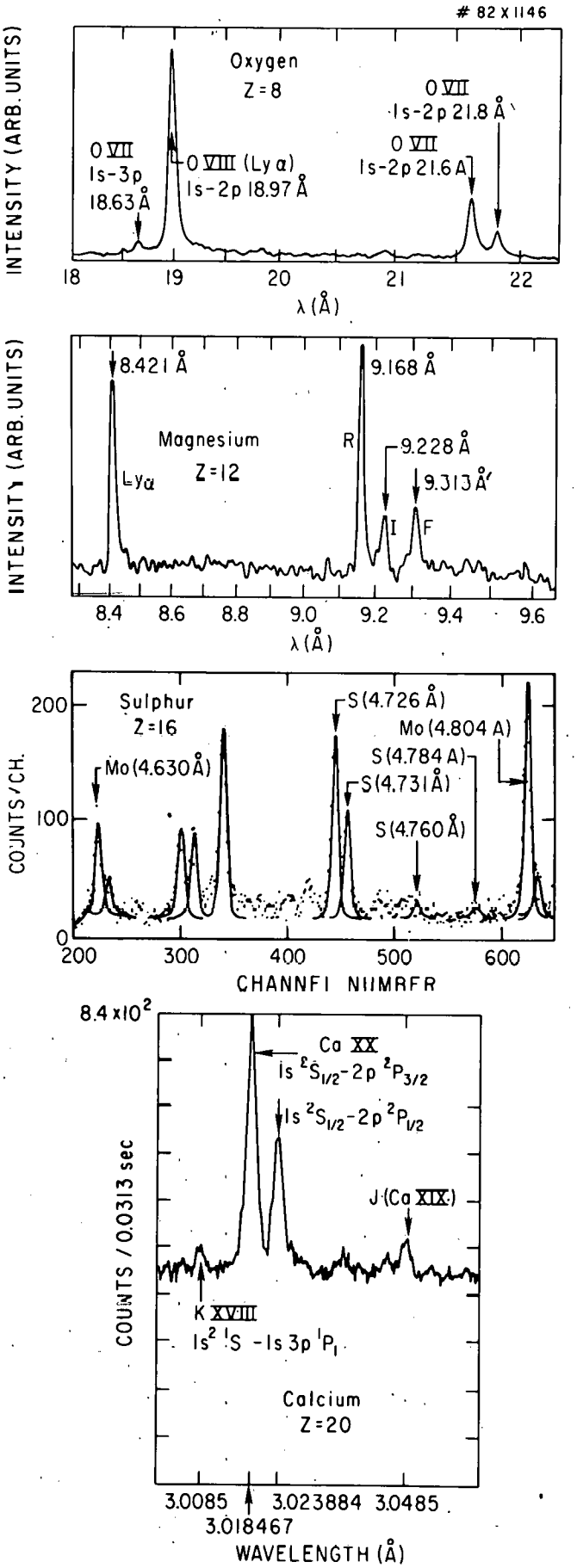
82 X 1146
Oxygen
Z=8
O VII
1s-2p 21.8 Å
O VII
1s-3p
18.63 Å
O VIII (Lyα)
1s-2p 18.97 Å
O VII
1s-2p 21.6 Å
INTENSITY (ARB. UNITS)
18
19
20
21
22
λ (Å)
8.421 Å
9.168 Å
Magnesium
Z=12
Lyα
R
9.228 Å
9.313 Å
I
F
INTENSITY (ARB. UNITS)
8.4
8.6
8.8
9.0
9.2
9.4
9.6
λ (Å)
Sulphur
Z=16
S(4.726 Å)
Mo(4.804 A)
S(4.784 A)
Mo(4.630Å)
S(4.731Å)
S(4.760Å)
COUNTS/CH.
200
100
0
200
300
400
500
600
CHANNEL NUMBER
8.4 x10²
Ca XX
1s ²S1/2-2p ²P3/2
1s ²S1/2-2p ²P1/2
J (Ca XIX)
K XVIII
1s² ¹S -1s3p ¹P1
Calcium
Z=20
COUNTS / 0.0313 sec
3.0085
3.023884
3.0485
3.018467
WAVELENGTH (Å)

Fig. 5

#83X0290

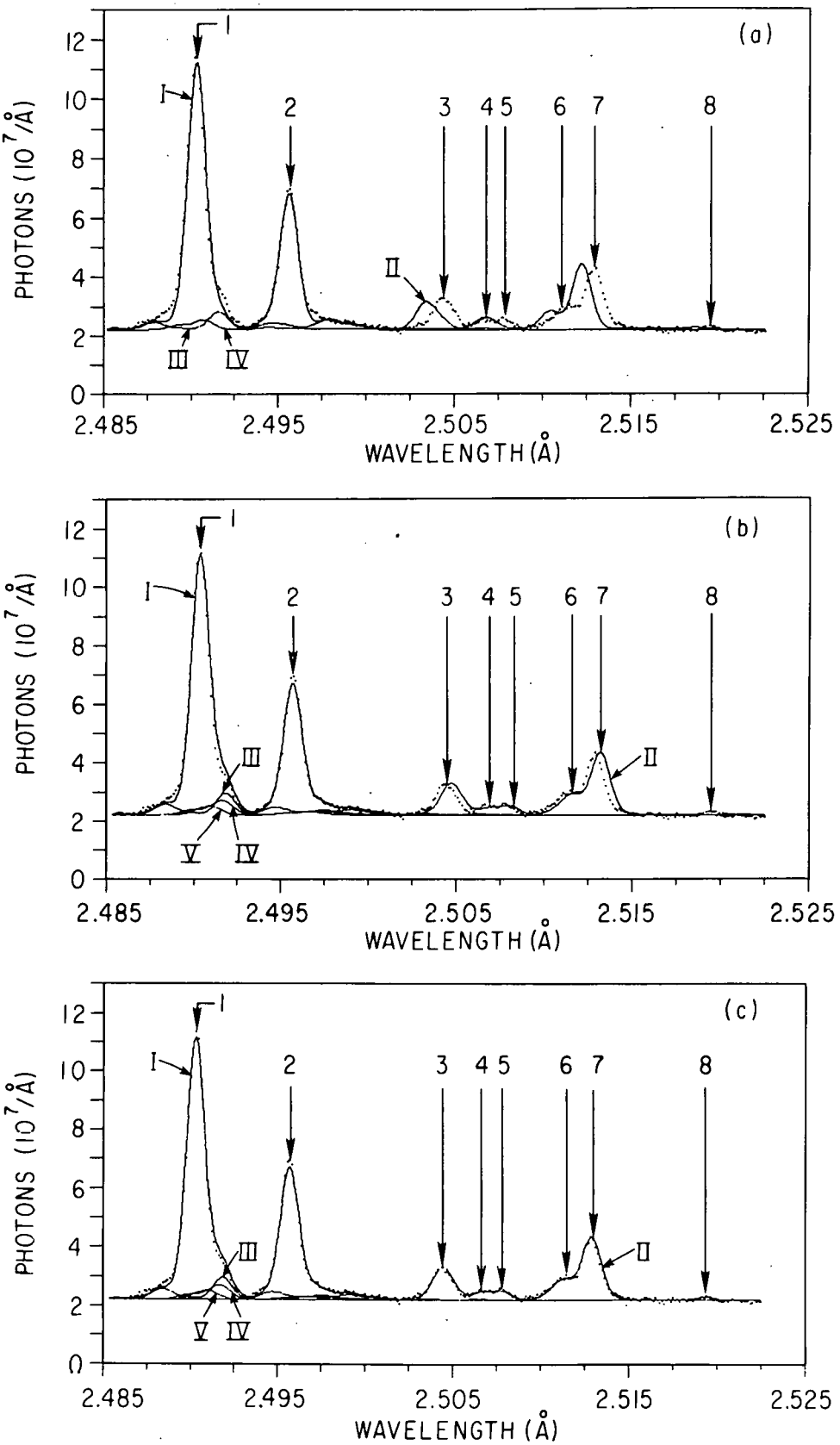

Fig. 6

#83X0440

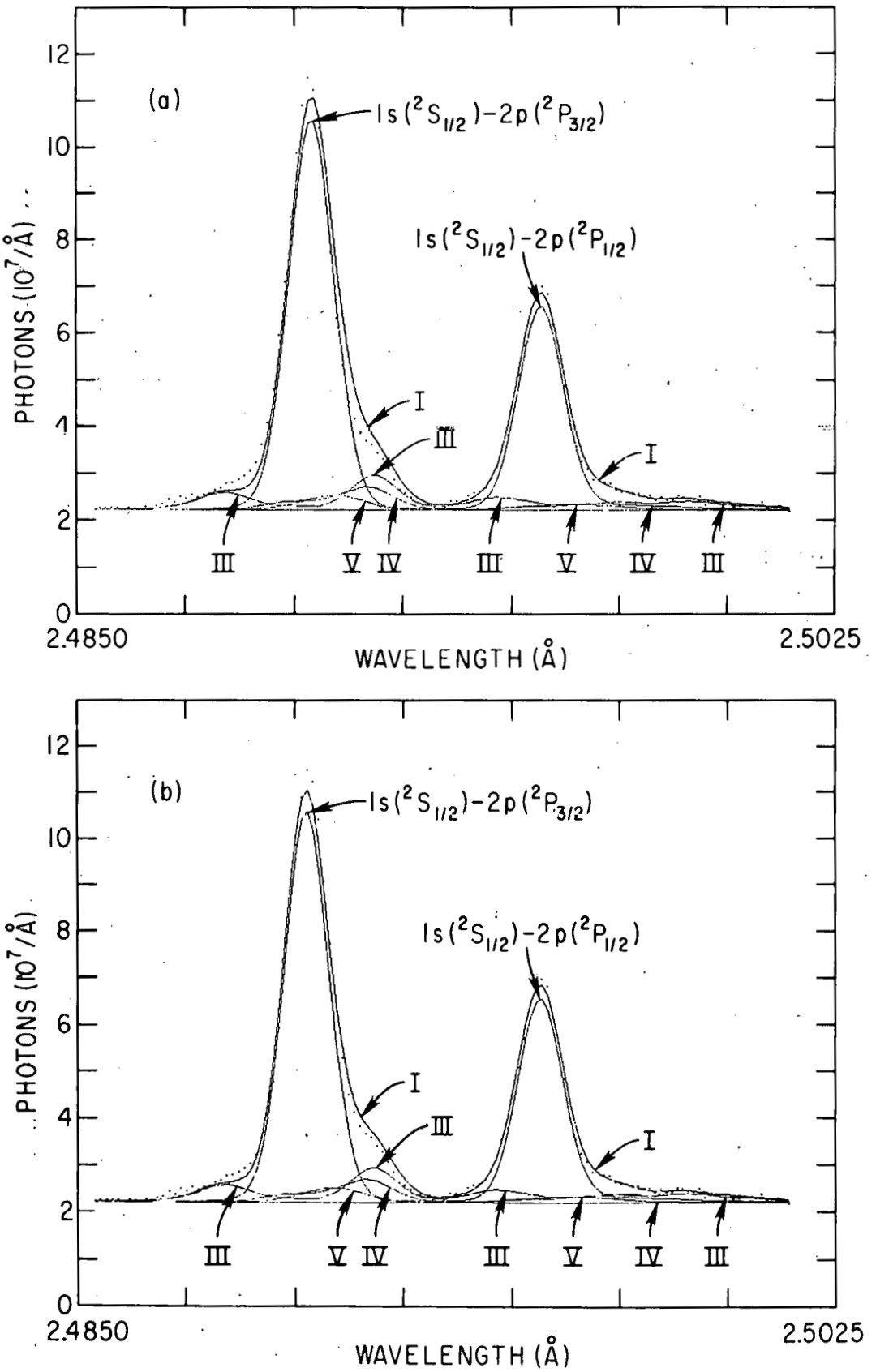

Fig. 7

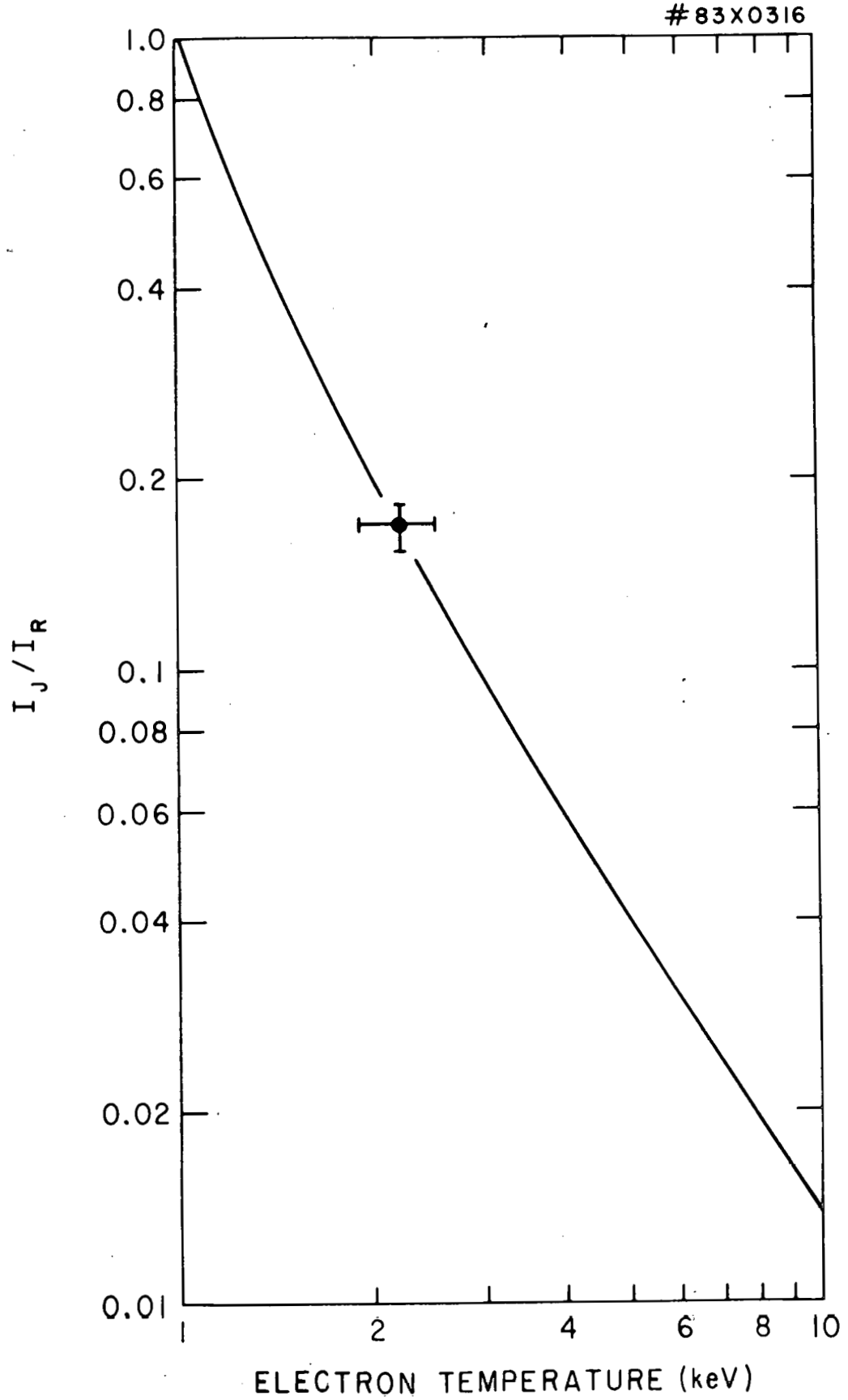
#83X0316
1.0
0.8
0.6
0.4
0.2
0.1
0.08
0.06
0.04
0.02
0.01
I_J/I_R
1
2
4
6
8
10
ELECTRON TEMPERATURE (keV)

Fig. 8

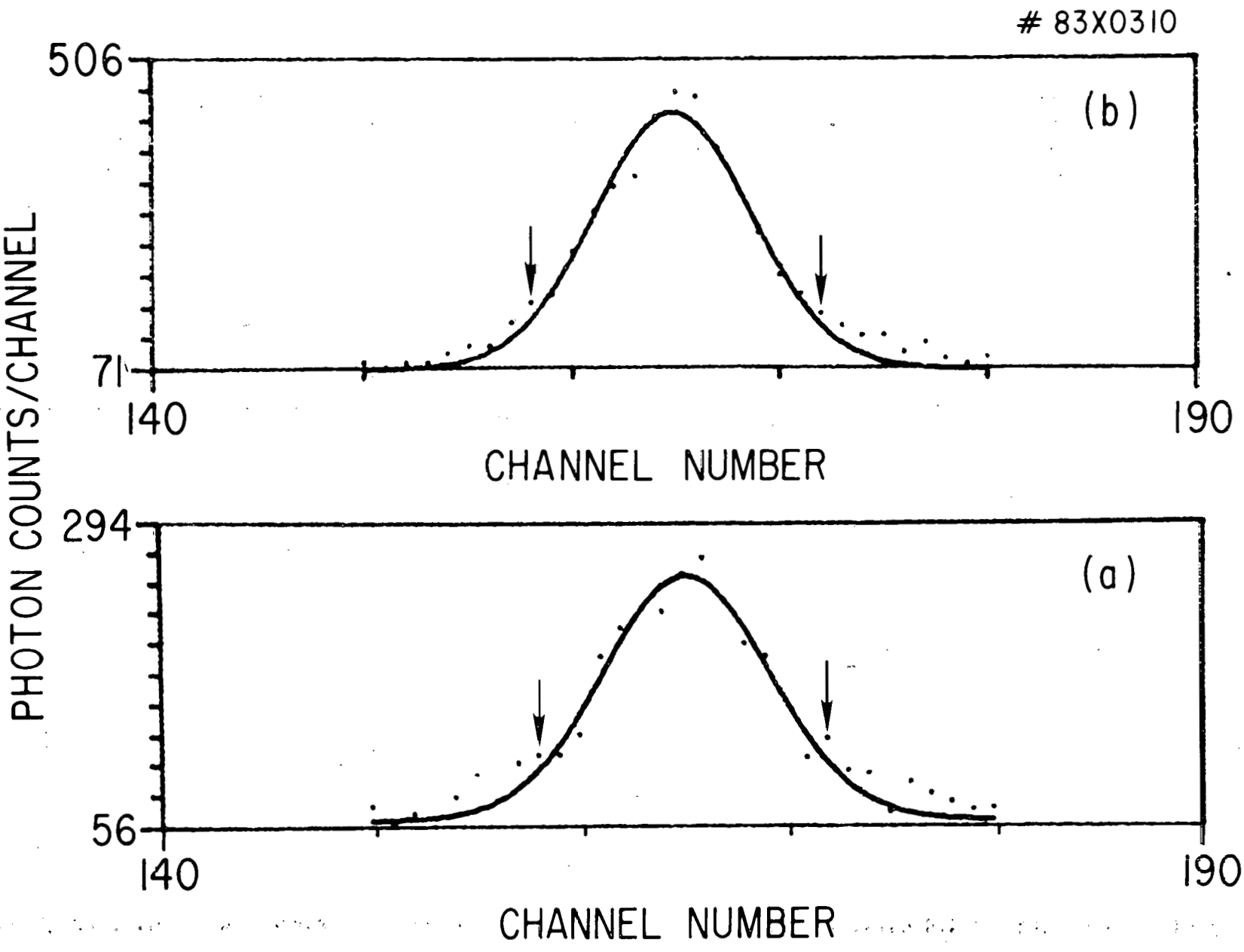
83X0310
506
71
(b)
140
190
CHANNEL NUMBER
294
56
(a)
140
190
CHANNEL NUMBER
PHOTON COUNTS/CHANNEL

Fig. 9

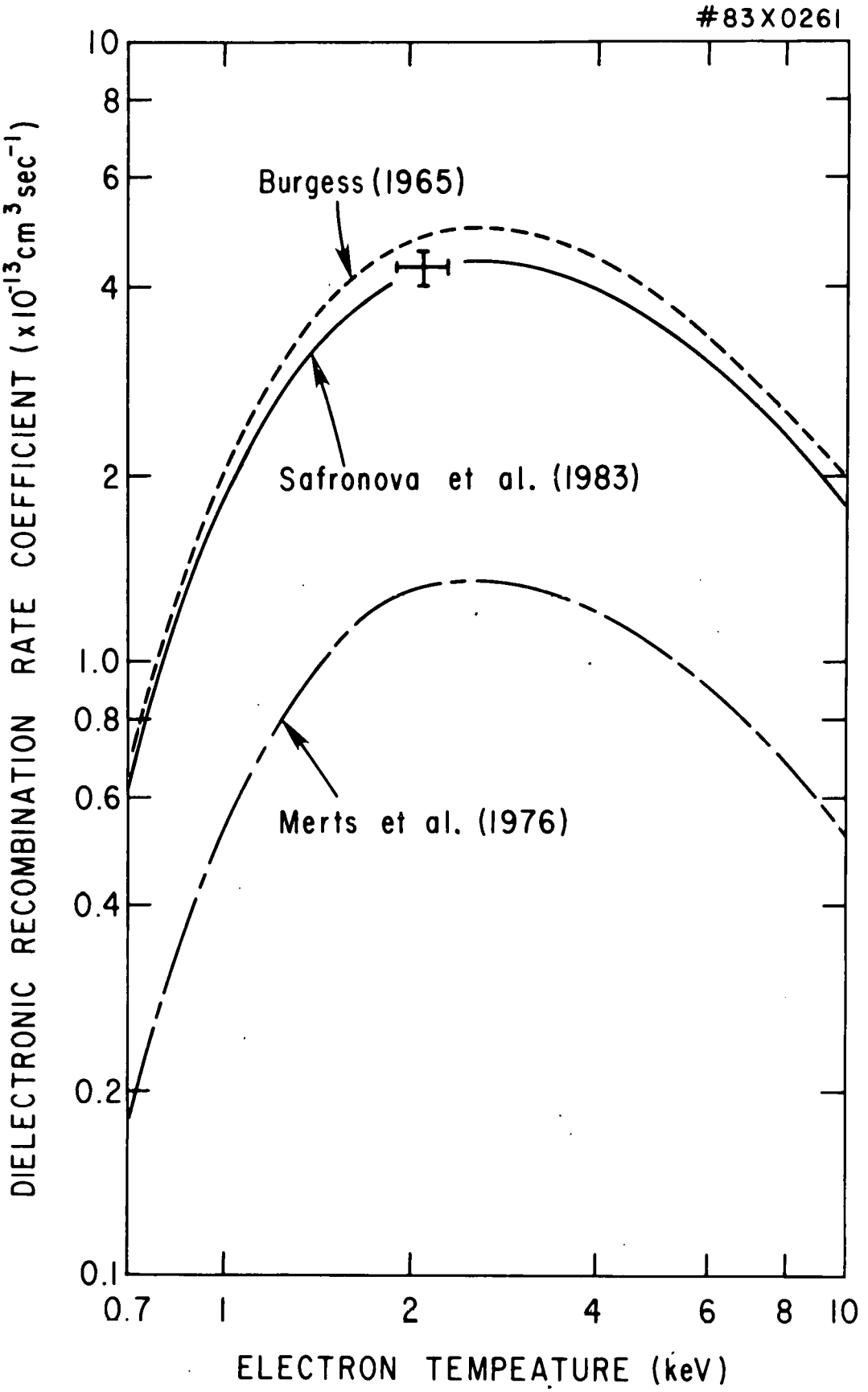
#83X0261
DIELECTRONIC RECOMBINATION RATE COEFFICIENT (x10^-13 cm^3 sec^-1)
10
8
6
4
2
1.0
0.8
0.6
0.4
0.2
0.1
Burgess (1965)
Safronova et al. (1983)
Merts et al. (1976)
0.7
1
2
4
6
8
10
ELECTRON TEMPEATURE (keV)

Fig. 10

EXTERNAL DISTRIBUTION IN ADDITION TO TIC UC-20

Plasma Res Lab, Austra Nat'l Univ, AUSTRALIA
Dr. Frank J. Paoloni, Univ of Wollongong, AUSTRALIA
Prof. I.R. Jones, Flinders Univ., AUSTRALIA
Prof. M.H. Brennan, Univ Sydney, AUSTRALIA
Prof. F. Cap, Inst Theo Phys, AUSTRIA
Prof. Frank Verheest, Inst theoretische, BELGIUM
Dr. D. Palumbo, Dg XII Fusion Prog, BELGIUM
Ecole Royale Militaire, Lab de Phys Plasmas, BELGIUM
Dr. P.H. Sakanaka, Univ Estadual, BRAZIL
Dr. C.R. James, Univ of Alberta, CANADA
Prof. J. Teichmann, Univ of Montreal, CANADA
Dr. H.M. Skarsgard, Univ of Saskatchewan, CANADA
Prof. S.R. Sreenivasan, University of Calgary, CANADA
Prof. Tudor W. Johnston, INRS-Energie, CANADA
Dr. Hannes Barnard, Univ British Columbia, CANADA
Dr. M.P. Bachynski, MPB Technologies, Inc., CANADA
Zhengwu LI, SW Inst Physics, CHINA
Library, Tsing Hua University, CHINA
Librarian, Institute of Physics, CHINA
Inst Plasma Phys, SW Inst Physics, CHINA
Dr. Peter Lukac, Komenskeho Univ, CZECHOSLOVAKIA
The Librarian, Culham Laboratory, ENGLAND
Prof. Schatzman, Observatoire de Nice, FRANCE
J. Radet, CEN-BP6, FRANCE
AM Dupas Library, AM Dupas Library, FRANCE
Dr. Tom Mual, Academy Bibliographic, HONG KONG
Preprint Library, Cent Res Inst Phys, HUNGARY
Dr. A.K. Sundaram, Physical Research Lab, INDIA
Dr. S.K. Trehan, Panjab University, INDIA
Dr. Indra, Mohan Lal Das, Banaras Hindu Univ, INDIA
Dr. L.K. Chavda, South Gujarat Univ, INDIA
Dr. R.K. Chhajlani, Var Ruchi Marg, INDIA
P. Kaw, Physical Research Lab, INDIA
Dr. Phillip Rosenau, Israel Inst Tech, ISRAEL
Prof. S. Cuperman, Tel Aviv University, ISRAEL
Prof. G. Rostagni, Univ Di Padova, ITALY
Librarian, Int'l Ctr Theo Phys, ITALY
Miss Clelia De Palo, Assoc EURATOM-CNEN, ITALY
Biblioteca, del CNR EURATOM, ITALY
Dr. H. Yamato, Toshiba Res & Dev, JAPAN
Prof. M. Yoshikawa, JAERI, Tokai Res Est, JAPAN
Prof. T. Uchida, University of Tokyo, JAPAN
Research Info Center, Nagoya University, JAPAN
Prof. Kyoji Nishikawa, Univ of Hiroshima, JAPAN
Prof. Sigeru Mori, JAERI, JAPAN
Library, Kyoto University, JAPAN
Prof. Ichiro Kawakami, Nihon Univ, JAPAN
Prof. Satoshi Itoh, Kyushu University, JAPAN
Tech Info Division, Korea Atomic Energy, KOREA
Dr. R. England, Ciudad Universitaria, MEXICO
Bibliotheek, Fom-Inst Voor Plasma, NETHERLANDS
Prof. B.S. Liley, University of Waikato, NEW ZEALAND
Dr. Suresh C. Sharma, Univ of Calabar, NIGERIA
Prof. J.A.C. Cabral, Inst Superior Tech, PORTUGAL
Dr. Octavian Petrus, ALI CUZA University, ROMANIA
Dr. R. Jones, Nat'l Univ Singapore, SINGAPORE
Prof. M.A. Hellberg, University of Natal, SO AFRICA
Dr. Johan de Villiers, Atomic Energy Bd, SO AFRICA
Dr. J.A. Tagle, JEN, SPAIN
Prof. Hans Wilhelmson, Chalmers Univ Tech, SWEDEN
Dr. Lennart Stenflo, University of UMEA, SWEDEN
Library, Royal Inst Tech, SWEDEN
Dr. Erik T. Karlson, Uppsala Universitet, SWEDEN
Centre de Recherchesen, Ecole Polytech Fed, SWITZERLAND
Dr. W.L. Weise, Nat'l Bur Stand, USA
Dr. W.M. Stacey, Georg Inst Tech, USA
Dr. S.T. Wu, Univ Alabama, USA
Prof. Norman L. Oleson, Univ S Florida, USA
Dr. Benjamin Ma, Iowa State Univ, USA
Prof. Magne Kristiansen, Texas Tech Univ, USA
Dr. Raymond Askew, Auburn Univ, USA
Dr. V.T. Tolok, Kharkov Phys Tech Ins, USSR
Dr. D.D. Ryutov, Siberian Acad Sci, USSR
Dr. M.S. Rabinovich, Lebedev Physical Inst, USSR
Dr. G.A. Eliseev, Kurchatov Institute, USSR
Dr. V.A. Glukhikh, Inst Electro-Physical, USSR
Prof. T.J. Boyd, Univ College N Wales, WALES
Dr. K. Schindler, Ruhr Universitat, W. GERMANY
Nuclear Res Estab, Julich Ltd, W. GERMANY
Librarian, Max-Planck Institut, W. GERMANY
Dr. H.J. Kaeppler, University Stuttgart, W. GERMANY
Bibliothek, Inst Plasmaforschung, W. GERMANY